

## Discovery of Benzo[cd]indol-2(1H)-ones as Potent and Specific BET Bromodomain Inhibitors: Structure-Based Virtual Screening, Optimization, and Biological Evaluation

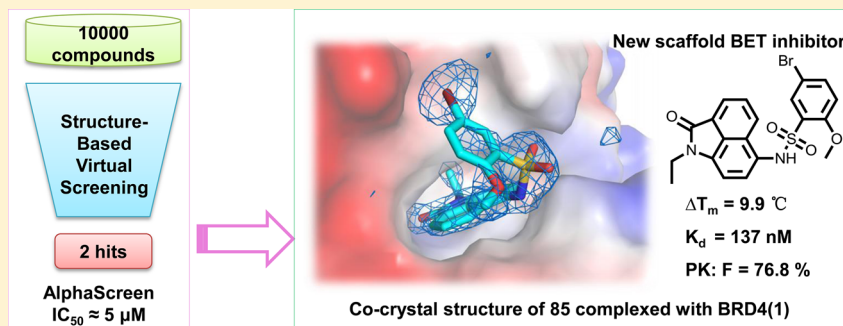
Xiaoqian Xue,<sup>†,‡,||</sup> Yan Zhang,<sup>†,||</sup> Zhaoxuan Liu,<sup>†,§,||</sup> Ming Song,<sup>†</sup> Yanli Xing,<sup>†,§</sup> Qiuping Xiang,<sup>†,‡</sup> Zhen Wang,<sup>†</sup> Zhengchao Tu,<sup>†</sup> Yulai Zhou,<sup>§</sup> Ke Ding,<sup>†</sup> and Yong Xu<sup>\*,†</sup>

<sup>†</sup>Institute of Chemical Biology, Guangzhou Institutes of Biomedicine and Health, Chinese Academy of Sciences, No. 190 Kaiyuan Avenue, Guangzhou Science Park, Guangzhou, Guangdong 510530, China

<sup>‡</sup>University of Chinese Academy of Sciences, No. 19 Yuquan Road, Beijing 100049, China

<sup>§</sup>Department of Bioengineering School of Pharmaceutical Sciences, Jilin University, No. 1266 Fujin Road, Chaoyang District, Changchun, Jilin 130021, China

### Supporting Information



**ABSTRACT:** The discovery of inhibitors of bromodomain and extra terminal domain (BET) has achieved great progress, and at least seven inhibitors have progressed into clinical trials for the treatment of cancer or inflammatory diseases. Here, we describe the identification, optimization, and evaluation of benzo[cd]indol-2(1H)-one containing compounds as a new class of BET bromodomain inhibitors, starting from structure-based virtual screening (SBVS). Through structure-based optimization, potent compounds were obtained with significantly improved activity. The two most potent compounds bind to the BRD4 bromodomain, with  $K_d$  values of 124 and 137 nM. Selected compounds exhibited high selectivity over other non-BET subfamily members. Notably, compound 85 demonstrated a reasonable antiproliferation effect on MV4;11 leukemia cells and exhibited a good pharmacokinetic profile with high oral bioavailability (75.8%) and moderate half-life ( $T_{1/2} = 3.95$  h). The resulting lead molecule 85 represents a new, potent, and selective class of BET bromodomain inhibitors for the development of therapeutics to treat cancer and inflammatory diseases.

### 1. INTRODUCTION

Acetylation of lysine residues is a post-translational modification that plays a key role in the regulation of the chromatin structure and transcription.<sup>1,2</sup> These changes in histone and their effect on gene expression are regulated by three categories of regulatory proteins, “writers”, “erasers”, and “readers”. Histone acetyltransferases (HATs) act as a writer to add an acetyl group to form an acetylated lysine, whereas histone deacetylases (HDACs) act as an eraser to remove the acetyl group from acetylated lysine. The bromodomain (BRD) family of proteins recognizes and binds to the acetylated lysine acting as a reader of lysine acetylation state.<sup>3,4</sup>

The bromodomain was named after it was first identified in the *Brahma* gene from *Drosophila melanogaster* as a protein domain containing approximately 110 amino acids.<sup>5</sup> There are 61 human bromodomains that are found within 46 proteins in

the human genome. These bromodomain-containing proteins can be divided into eight diverse bromodomain groups.<sup>2,4</sup> Structural studies have revealed that bromodomains have a conserved structural fold which consists of a left-handed four-helix bundle and two interspersed ZA and BC loops which constitute the active acetyl lysine-binding pocket (Figure S1).<sup>2,6,7</sup> The site contains an evolutionarily conserved asparagine side chain that acts as a hydrogen bond donor to the acetylated lysine side chain. A second interaction occurs between the acetyl carbonyl oxygen atom and the phenol of a conserved tyrosine via a structured water molecule. Despite this conserved overall structure, different bromodomains recognize

**Special Issue:** Epigenetics

**Received:** September 29, 2015

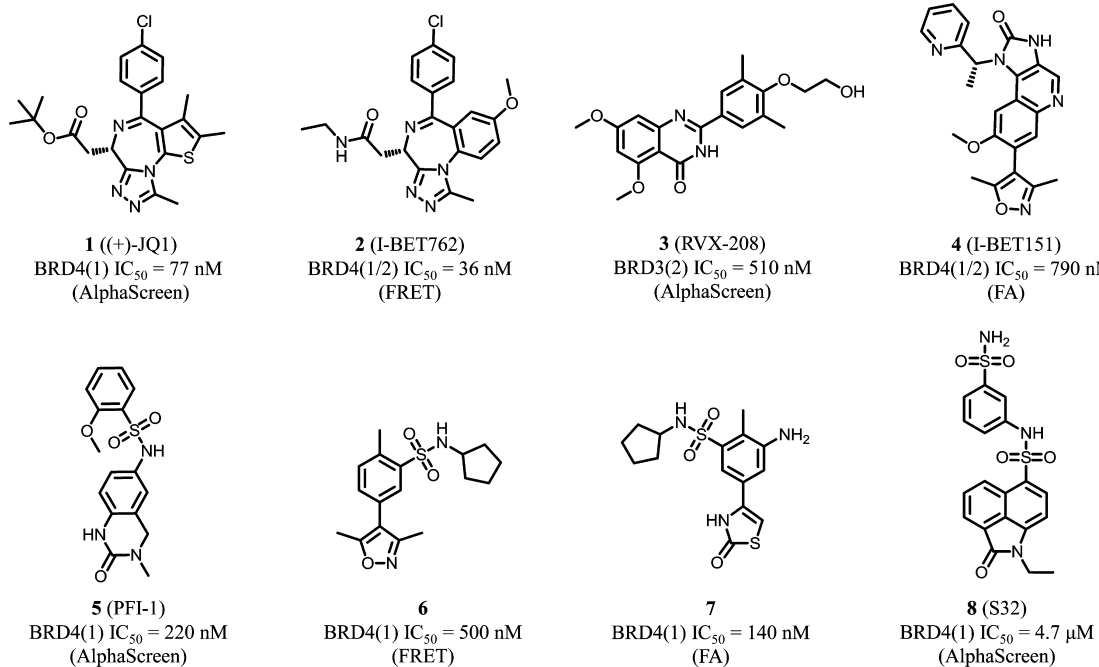


**Figure 1.** Structures of representative bromodomain inhibitors.  $IC_{50}$  values for the inhibitors are shown with the method used.

distinct acetylated lysines in different proteins because the specific amino acid residues within the loops of each bromodomain are critical for determining the acetyl lysine-binding specificity. The architecture of their acetylated lysine binding pocket makes them attractive targets for the development of potent and specific inhibitors. Bromodomain-containing proteins have been implicated in the development of diverse diseases such as cancer and inflammation.<sup>8–15</sup>

Recently, a number of small-molecule compounds with potent inhibitory activity against bromodomain family proteins were reported in the literature.<sup>16–21</sup> Known bromodomain inhibitors mainly target the BET subfamily, including BRD2, BRD3, BRD4, and BRDT. The first potent BET inhibitors reported were the diazepines **1** ((+)-JQ1) and **2** (I-BET762) (Figure 1).<sup>8,22</sup> **1** was obtained after the simple modification of the BRD4 inhibitors patented by Mitsubishi Pharmaceuticals, and **2**, as reported by Nicodeme et al., was derived from medicinal chemistry optimization of a hit derived from a phenotypic screen designed to identify small molecules able to enhance ApoA1 expression. **2** has entered clinical trials for NUT midline carcinoma. The quinolinone-base compound **3** (RVX-208, Figure 1), which was initially described as a compound that upregulated ApoA1 expression and increased the high-density lipoprotein mass in vitro and in vivo, has recently been reported to be a BET inhibitor.<sup>15</sup> GSK has also reported the isoxazoloquinoline derivative **4** (I-BET151, Figure 1) as a BET inhibitor and has demonstrated efficacy in studies of MLL-fusion leukemia.<sup>23,24</sup> The dihydroquinazolinone **5** (PFI-1, Figure 1) was recently reported to be a BET chemical probe derived from the optimization of a fragment-screening hit.<sup>13,25</sup> The compound exhibits modest activity against cell lines carrying oncogenic rearrangements in the MLL locus, although its solubility and pharmacokinetics are suboptimal.

Fragment-based screening methods have been extensively used to identify BET inhibitors for different chemotypes. Most of the compounds reported in these studies are generally weak inhibitors but represent promising starting points for further

medicinal chemistry optimization. Chung et al. identified a weak fragment inhibitor and obtained a potent and selective sulfonamide inhibitor **6** (Figure 1) with an  $IC_{50}$  of 500 nM through extensive medicinal chemistry optimization.<sup>26,27</sup> Zhao et al. found that thiazolidinone could mimic an acetylated lysine moiety and bind to BRD4 protein. Further optimization led to a potent BRD4 inhibitor **7** (Figure 1) with an  $IC_{50}$  of 140 nM and favorable metabolic stability.<sup>28,29</sup> Gehling et al. at Constellation Pharmaceuticals reported isoxazole-based BET bromodomain inhibitor developed using hits from a fragment screening. Further optimization led to its carboxamide derivative with an  $IC_{50}$  value of 26 nM against BRD4(1) in the AlphaScreen assay.<sup>30</sup>

Rapid progress in the development of bromodomain ligands has stimulated extensive interest and has led to at least seven BET bromodomain inhibitors reaching clinical trials.<sup>31,32</sup> However, the chemotypes are still limited. The discovery of new potent and specific BET inhibitors with improved pharmacokinetics and physicochemical properties will greatly enhance our understanding of the therapeutic potential of bromodomain inhibition for various human diseases.

In the present work, we report a structure-based virtual screening combined with free energy evaluation, medicinal chemistry optimization, and biological evaluation of a new class of potent, specific and bioavailable small-molecular BET inhibitors, the benzo[cd]indol-2(1H)-ones.

## 2. RESULTS AND DISCUSSION

### 2.1. Identification and Validation of Benzo[cd]indol-2(1H)-one Scaffold by Structure-Based Virtual Screening.

Virtual screening is a powerful tool for novel scaffold discovery. In this study, a common virtual screening strategy was used as shown in Figure 2. Our in-house library with approximately 10000 compounds was screened through molecular docking and binding free energy evaluation. After cluster analysis and visual inspection, 15 representative compounds were selected for biological assays (Supporting

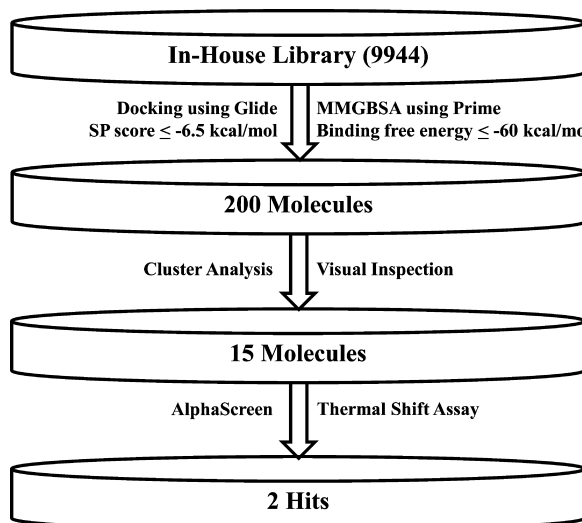


**Figure 2.** Schematic representation of the virtual screening strategy used for BRD4(1) inhibitor discovery.

Information, Figure S2). Using a thermal shift assay, 7 of the 15 compounds demonstrated a stabilized effect for BRD4(1) protein with a temperature shift of more than 1.0 °C (Supporting Information, Table S1). The AlphaScreen assay further demonstrated that two of the compounds (8 (S32), *N*-(4-(1-ethyl-2-oxo-1,2-dihydrobenzo[*cd*]indole-6-sulfonamido)-phenyl)acetamide (S35)) showed low micromolar level activity with IC<sub>50</sub> values of 6.93 and 4.70 μM, respectively. The corresponding ligand efficiencies were approximately 0.25. These two compounds bearing a benzo[*cd*]indol-2(1*H*)-one scaffold were previously used as nuclear receptor inhibitors and plant hormone receptor agonists in our previous studies.<sup>33,34</sup>

To design more potent derivatives, we compared the binding mode of 1 and 8 bound to BRD4(1) (Figure 1, Figure 3A,B). The binding mode predicted by molecular docking study demonstrated that compound 8 binds snugly in the acetyl lysine binding site. The carbonyl oxygen atom of the amide group interacts with the conserved residues Asn140 and Tyr97 through direct and indirect hydrogen bonds via a water molecule, respectively. The ethyl group attached to the amide group mimicked the terminal methyl group of the acetyl lysine and occupied the small pocket surrounded by residues Pro82, Phe83, Val87, and Ile146. The planar benzo[*cd*]indol-2(1*H*)-one scaffold binds to and forms extensive hydrophobic interactions with the deep and narrow acetyl lysine binding pocket. N-Substitution of the sulfonamide group occupied the

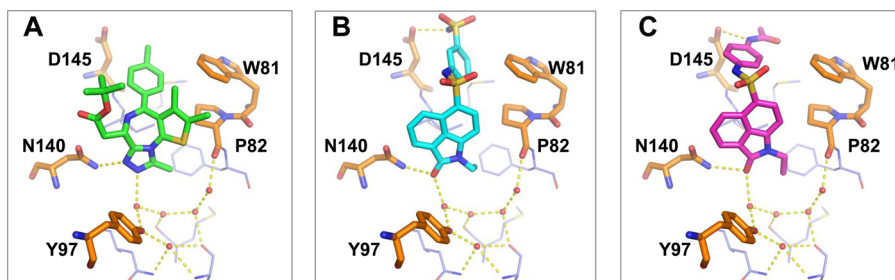
hydrophobic WPF shelf through the sulfonamide bend angle. The sulfonamide group at the 3-position of *N*-benzyl sulfonamide forms one more hydrogen bond with residue Asp145. To investigate the complex stability, molecular dynamic simulations were performed. The results demonstrated that the 8-BRD4(1) complex is very stable with a RMSD values of approximately 2 Å for all protein atoms and approximately 1 Å for the ligand during a 20 ns simulation time (Supporting Information, Figure S3). These important interactions mentioned above were maintained during the simulation, which validated that the predicted binding mode is rational and can be used for hit optimization. Therefore, we are confident that we can design and optimize the ligand based on the predicted mode.

To develop compounds with improved affinity for BRD4(1), we focused on two regions to perform an extensive SAR study to enhance the protein–ligand interactions. The first region is the hydrophobic WPF shelf, and the second region is the small binding portion of acetyl lysine tail.

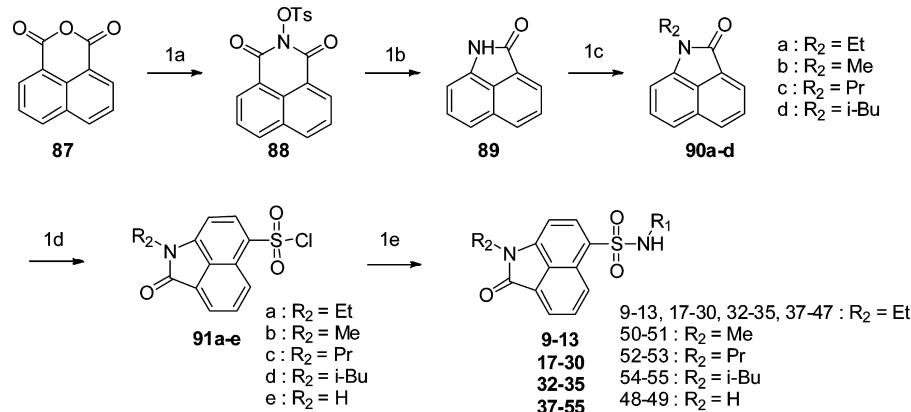
**2.2. Chemistry.** The sulfonamide derivatives of benzo[*cd*]-indol-2(1*H*)-one were designed and synthesized as shown in Scheme 1. The commercially available benzo[*de*]isochromene-1,3-dione (87) reacted with hydroxylamine hydrochloride and PTSA in the presence of pyridine to produce compound 88, which was then reacted with NaOH followed by HCl treatment to produce benzo[*cd*]indol-2(1*H*)-one (89). Alkyl substitution products (90a–d) were obtained by addition of iodoalkane or bromoalkane. The sulfonyl chloride substitution products (91a–e) were obtained through chlorosulfonic acid. Treatment of different amine compounds in the presence of organic bases gave the desired sulfonamide products 9–13, 17–30, 32–35, and 37–55.

The reversed sulfonamide derivatives of benzo[*cd*]indol-2(1*H*)-one were designed and synthesized as shown in Scheme 2. 1-Ethylbenzo[*cd*]indol-2(1*H*)-one (90a) was reacted with nitric acid and acetic acid to produce nitro-substitution product (92). Nitro reduction was achieved through iron and ammonium chloride. The reversed sulfonamide products 56–80, 82, and 84–86 were prepared from 6-amino-1-ethylbenzo[*cd*]indol-2(1*H*)-one and commercially available sulfonyl chlorides.

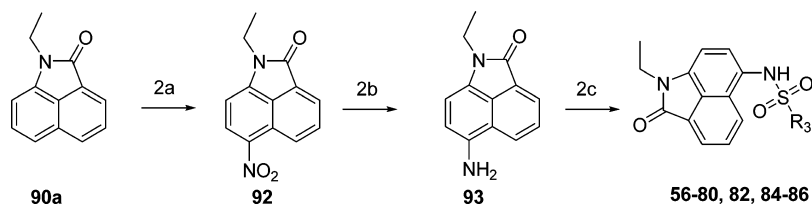
Compounds 14, 36, 81, and 83 were synthesized by simple hydrolysis reaction (Supporting Information, Scheme S1). Compound 31 was synthesized by addition of trifluoroacetic acid (TFA) to remove the *t*-butyloxycarbonyl group of compound 39 (Supporting Information, Scheme S2) (for details, see Supporting Information).



**Figure 3.** Binding modes of ligands with BRD4(1) protein. (A) Cocrystal structure of 1 in complex with BRD4(1) protein (PDB ID: 3MXF). (B) Predicted binding mode of 8 in complex with BRD4(1) protein. (C) Predicted binding mode of compound S35 complexed with BRD4(1). The ligands and important residues are shown as stick. Water molecules are shown as red spheres. The hydrogen bonds are shown as yellow dashed lines. Figures were prepared using PyMOL.

**Scheme 1.** Synthesis of Benzo[cd]indol-2(1H)-one Derivatives with a Sulfonamide Linker<sup>a</sup>

<sup>a</sup>Reagents and conditions: (1a) NH<sub>4</sub>OH·HCl, pyridine, PTSA, 95 °C, 1 h; (1b) (i) 2.7 mol/L NaOH, EtOH, H<sub>2</sub>O, reflux, 3 h, (ii) HCl, rt, 30 min; (1c) K<sub>2</sub>CO<sub>3</sub>, iodoalkane or bromoalkane, DMF, 50 °C, overnight; (1d) HSO<sub>3</sub>Cl, CHCl<sub>3</sub>, 0–50 °C, 6.0 h; (1e) R<sub>2</sub>-NH<sub>2</sub>, pyridine, 80 °C, 1 h or R<sub>2</sub>-NH<sub>2</sub>, DIPEA, DCM, rt, 3 h.

**Scheme 2.** Synthesis of Benzo[cd]indol-2(1H)-one Derivatives with a Reversed Sulfonamide Linker<sup>a</sup>

<sup>a</sup>Reagents and conditions: (2a) HNO<sub>3</sub>, acetic acid, 0–50 °C, 1 h; (2b) Fe, NH<sub>4</sub>Cl, acetic acid, H<sub>2</sub>O, 50 °C, 20 min; (2c) R<sub>1</sub>SO<sub>2</sub>Cl, CH<sub>2</sub>Cl<sub>2</sub>, pyridine, rt, 2 h.

### 2.3. Structure–Activity Relationships of N-Substituent Sulfonamide Derivatives of Benzo[cd]indol-2(1H)-one

To find more potent analogues based on the experimentally determined and modeled complex structures, we designed various substituents on the phenyl group to explore the chemical space for affinity improvement (Table 1). We preferentially evaluated the phenyl group and 4-chlorophenyl group, which are used in many potent molecules, such as 1. As shown in Figure 3B, the N-substituents sulfonamide of benzo[cd]indol-2(1H)-one could reach the WPF shelf and form favorable van der Waals interaction. Compound 9, with a phenyl group, is the most potent one ( $IC_{50} = 1.0 \mu\text{M}$  and  $\Delta T_m = 7.5^\circ\text{C}$ ) compared with other compounds that have a substituted phenyl group. Chloro-substituents at any position (10, 11, or 12) were tolerable and the corresponding compounds showed weaker activity than 9. For the polar substituent carboxy group, only the ortho-position compound 14 maintained the activity with an  $IC_{50}$  value of  $1.04 \mu\text{M}$  and a temperature shift of  $7.2^\circ\text{C}$  in the thermal shift assay. Compound 15, which bears a meta-position carboxy group showed moderate activity, whereas compound 16, which bears a para-position carboxy group, had no activity. The biochemical activity results showed that ortho-substituents on the ring were most favorable, whereas 13, which has an acetyl group at this position, was less potent, with a 3-fold decrease of activity. For para-position substituents, replacement of chlorine (10) with fluorine (17) resulted in a 2-fold increase of inhibitory activity, which suggests that the size of the substituent at the 4-position is important for compound activity. From the crystal structure of 17–BRD4(1) (Figure 4A, Supporting Information, Figure S4), we can see that the fluorine atom fit very well in the small

pocket, whereas 16, with the larger carboxy substituent, interfered with the protein.

To further explore SAR, hydrophobic and flexible groups were incorporated into the molecule (Table 2). These substituents made hydrophobic interactions with residues Ile146, Trp81, Pro82, Phe83, and Met149 in the WPF pocket entrance. When the substituents were alkyls, changing the chain from methyl to propyl, led to a significant potency improvement. However, further extension of the carbon chain gradually decreased the activity.

To understand the structural basis for the SAR, we determined the cocrystal structure of 19 bound to BRD4(1). As shown in Figure 4B, the amino of sulfonamide has H-bond interactions with a water molecule. This water molecule, along with other water molecules, mediated an H-bond network and formed H-bond interactions with Asp144 and Asp145. The crystal structure also revealed that the ethyl group well occupied the hydrophobic cavity, and the addition of an extra carbon atom in 20 resulted in greater potency. For comparison, we synthesized compounds containing polar group in the alkyl (26), which showed a significant loss of inhibition. However, the incorporation of a boc amino group in the butane chain (25) showed moderate activity.

When cycloalkyl groups were used to occupy the hydrophobic pocket, a large increase in inhibition was found. Among them, analogue 28 was one of the best compounds with strong biochemical activity ( $\Delta T_m = 10.5^\circ\text{C}$ ;  $IC_{50} = 0.13 \mu\text{M}$ ). Expanding the size to cycloheptane (29, Figure 4D) resulted in 3.5-fold decreased activity, which suggests that the optimal length of the substitution is approximately 2–4 heavy atoms. The crystal structure of 28 (Figure 4C) showed its binding

**Table 1.** Structure–Activity Relationship of the N-Phenyl Sulfonamide Derivatives of Benzo[cd]indol-2(1H)-one

No.	R <sub>1</sub>	AlphaScreen ( $\mu\text{M}$ ) <sup>a</sup>	TSA $\Delta T_m$ (°C) <sup>b</sup>	cLogP <sup>c</sup>	LE <sup>d</sup>
<b>1</b>		0.12±0.01	12.0	4.82	0.31
<b>9</b>		1.00±0.12	7.5	3.09	0.34
<b>10</b>		3.24±0.19	3.6	3.88	0.30
<b>11</b>		3.74±0.74	3.7	3.88	0.29
<b>12</b>		1.96±0.10	5.1	3.32	0.31
<b>13</b>		15.1±1.48	2.1	3.09	0.24
<b>14</b>		1.04±0.08	7.2	3.55	0.30
<b>15</b>		6.49±0.33	2.5	2.92	0.26
<b>16</b>		>30	0.0	2.92	<0.23
<b>17</b>		1.53±0.22	6.8	3.31	0.31

<sup>a</sup>The IC<sub>50</sub> was calculated from the AlphaScreen assay. The data were expressed as the means ± SD, representing the data from at least three independent experiments. <sup>b</sup>The  $\Delta T_m$  values were calculated from the thermal shift assay. <sup>c</sup>cLogP values were calculated using ChemBiodraw Ultra12.0. <sup>d</sup>Ligand efficiency (LE) = 1.4 (pIC<sub>50</sub>/heavy atoms).

mode similar to **19** (Figure 4B). To confirm the importance of hydrophobic interactions, we synthesized compounds with polar atoms in the cycloalkyl group (**30**, **31**, and **32**). The results demonstrated that including polar atoms reduced the inhibitory activity. For example, if the substituent atom is N (**31**), a loss of inhibition was observed, and the O analogue (**30**) was better than the N analogue. Compounds **35** and **36** showed moderate activity, which is consistent with analogue **14** and can be explained by the crystal structure of **36** (Figure 4E). When the carboxy group exposed to solvent was present, the water-mediated H-bond network was formed and provided less optimal arrangement (comparing with **28**). The water molecules form several H-bond interactions, with the carbonyl group of Asp145 and amino group of Ile146 on the main chain at the pocket entrance.

As mentioned above, **25** showed moderate activity. Considering the flexibility of **25**, we further synthesized conformational constraint analogues **37**, **38**, **39**, and **40**. Compounds **37** and **38** exhibited similar potency as **25**, whereas **39** and **40** showed a little decreased activity with IC<sub>50</sub> values of 4.10 and 4.84  $\mu\text{M}$ . Overall, the modification with substituents attached to cycloalkyls near the hydrophobic pocket did not improve the potency. Thereafter, flexible linkers with 1–3 methylenes were used to attach polar substituents for improved activity (**41**–**47**). However, these compounds exhibited moderate or weak activity. From the above SAR, we can see that the most potent compounds in this series are **20** and **28**.

As shown Figure 4C, in the cocrystal structure of **28** bound to BRD4(1) protein, a small subpocket exists near the ethyl portion of the pyrrolidin-2-one ring. There are two conserved water molecules in this subpocket. Oleg Fedorov et al. attempted to displace the water molecules with polar group but failed to do so.<sup>35</sup> To investigate a suitable substitution, the preferred butyl and cyclohexyl group was maintained in the R<sub>1</sub> position, and R<sub>2</sub> was replaced with hydrogen atoms or short-chain alkyl group (**48**–**55**). The activity demonstrated that ethyl is the best substituent. To rationalize this result, we superimposed two complexes of BRD4(1) with analogue **28** and acetylated lysine (Figure 5A). The ethyl group at the R<sub>2</sub> position is the optimal size and fit very well with the acetyl group of the acetylated lysine. A larger alkyl group may interfere with residues around this pocket.

#### 2.4. Structure–Activity Relationships of Reversed Sulfonamide Derivatives of Benzo[cd]indol-2(1H)-one.

The sulfonamide linker provides a suitable angle turn for N-substitution to reach into the hydrophobic pocket. To explore the chemical space, we also synthesized compounds with a reversed sulfonamide linker. We combined the reversed sulfonamide linker with the optimal alkyl and cycloalkyl motifs obtained above, leading to compounds **56**–**60**. These compounds displayed comparable inhibitory activity to BRD4(1). We solved the complex structure of **58** bound with BRD4(1). The structure (Figure 5B) showed that the NH of reversed sulfonamide linker formed an H-bond interaction with the solvent water. The existing water presented suitable geometry to enable good contact with two other waters. By comparing the crystal structures of **58** and **19** bound to BRD4(1) (Figure 5B), we found that the benzo[cd]indol-2(1H)-one scaffolds were overlapped in the KAc binding pocket. The turn angle of the reversed sulfonamide linker was larger than that of the sulfonamide linker, which resulted in the butyl motif of **58** being situated at the same position as the ethyl motif of **19**. The butyl analogue **58** (IC<sub>50</sub> = 0.73  $\mu\text{M}$ ) showed a slight increase in potency compared with its ethyl analogue **19** (IC<sub>50</sub> = 1.09  $\mu\text{M}$ ). By comparing the trends of activities for alkyl substituent compounds (**20** vs **57**, **21** vs **58**), we concluded that the optimal substituent was approximately three heavy atoms for sulfonamide analogues but five heavy atoms for reverse sulfonamide analogues. Similarly, the cycloalkyl analogue **60** (IC<sub>50</sub> = 0.21  $\mu\text{M}$ ) exhibited a slight potency decrease compared with compound **28** (IC<sub>50</sub> = 0.13  $\mu\text{M}$ ).

As shown in Figure 5B, the larger rotation angles of the reversed sulfonamide resulted in a shift of the substituent (**58** vs **19**). On the basis of the structure analysis, we next explored the attachment of benzyl groups with various substituents. When the substituent on the phenyl group was halogen, the compounds displayed moderate potency. The 4-chloro analogue **64** showed similar activity as that of **10**. The SAR of compounds **61**, **62**, and **63** were consistent with their analogues **12**, **11**, and **10**.

Various types of 4-substituent analogues were tested, and decreased BRD4(1) activity was observed compared with the 2-substituent compounds (**63**–**65**). Although no structural information is available for this series of compounds, we can conclude that the binding modes of these compounds are similar to that of **17** from molecular docking study.

As shown in Table 3, when using a benzyl group as the substituent, the flexibility of the molecule may be detrimental to its potency. We then investigated the effect of various

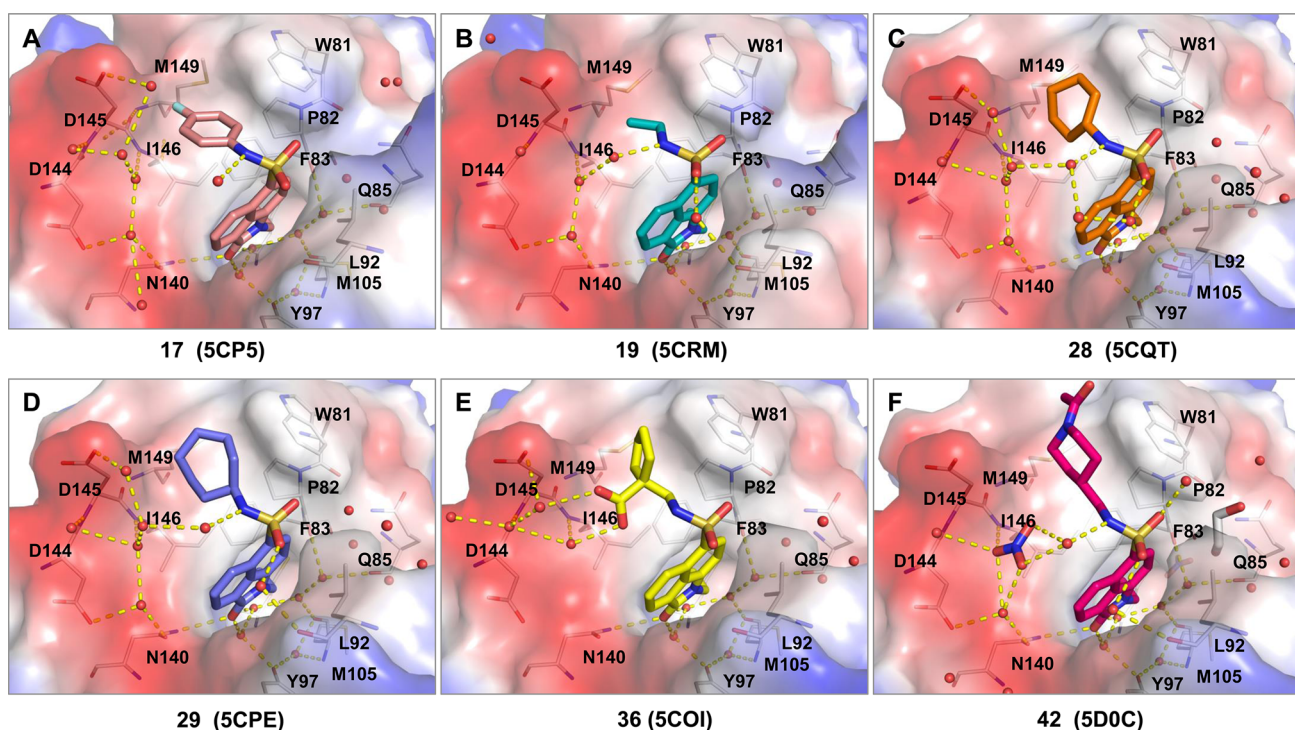


**Figure 4.** Cocrystal structures of compounds 17 (A), 19 (B), 28 (C), 29 (D), 36 (E), and 42 (F) with BRD4(1) (PDB IDs: 5CP5, 5CRM, 5CQT, 5CPE, 5COI, and 5D0C, respectively). The ligands are shown as sticks, and the protein is shown as a ribbon. The electrostatic potential surface is transparent for clarity. The binding site residues are shown as lines. Hydrogen bonds interactions are indicated by dashed lines in yellow. Compounds are well-defined by the electron density. Ligand-omitted electron density maps were included in the Supporting Information.

substitutions directly on the aromatic ring. The results for representative examples of R<sub>3</sub> modifications are summarized in Table 4. The thienyl derivative 66 and phenyl derivative 67 showed high binding affinity compared with the benzyl derivatives listed in Table 4. A monosubstituent on the phenyl group with halogen atoms (68, 69, and 70) led to a slight loss of activity compared with 67. This is consistent with those compounds with a sulfonamide linker listed in Table 1.

Similar to the above results, the unsubstituted phenyl ring (67) maintained the optimal activity compared to monosubstitution. However, the monosubstituted analogues with reverse sulfonamide linker were more tolerated than sulfonamide compounds. When two halogen atoms were added to the phenyl ring at different positions, improved potency was obtained. When fluorine atoms were presented as 2,4-substitutions, the activities were better than that of other dihalogen substituents. Among them, 73, which has a 2,4-difluoro-phenyl group, exhibited significantly improved activity, with an IC<sub>50</sub> of 0.12 μM. The TSA assay also demonstrated its effect of stabilizing the BRD4(1) protein with a temperature shift of 9.5 °C. From the data listed in Table 4, we can see that the steric and electronic properties were both important for improved activity. When 4-position substitutions were varied from fluorine (68) to methyl (77), the compound potency was maintained.

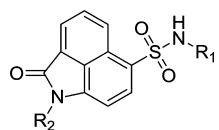
Different sized electron-withdrawing or electron-donating substitutions at 4-position including methyl, cyano, and nitro (77–79), exhibited only moderate activity with IC<sub>50</sub> values of approximately 1–5 μM. The crystal structure of 71 (Figure 5D) bound to BRD4(1) indicated that a size restriction exists in this area. Single atom substitution was most favorable in this direction.

For the sulfonamide derivatives described above, we investigated the effect for compounds with ortho-position substituents, which may form favorable interaction with surrounding water molecules. We use a similar strategy and synthesized compounds 80, 81, 82, and 83. No significant potency improvement was obtained for these compounds, although a water-bridged H-bond network was formed, as shown in the crystal structure of 80 bound to BRD4(1) protein (Figure 5E).

We superimposed the structure of compound 67 with that of the literature-reported active molecules. Surprisingly, the phenyl motif overlapped very well with that of 5. This discovery encouraged us to design 2-methoxy compounds. The 2,5-disubstituent derivative 85 exhibited a similar inhibitory activity to that of the unsubstituted 67, suggesting that H-bond interaction with the water is beneficial to maintaining activity. Replacement of 5-chloro (84) with 5-bromo (85) led to a slightly increased activity, whereas it reduced the activity compared with that of 5-methoxy substituted 86.

**2.5. Evaluation of Binding Affinity and Cell Growth Inhibition Activity.** To further confirm the binding abilities to BRD4(1), representative compounds were selected based on TSA and AlphaScreen assays. Isothermal titration calorimetry (ITC) experiments were performed and the K<sub>d</sub> values were determined and are listed in Table 5. Most of the tested compounds exhibited K<sub>d</sub> values in the nanomolar range. The results suggested that these compounds had good binding activities for BRD4(1), which were consistent with the data from the AlphaScreen and TSA assays. Compounds 28 and 85 were identified as the most active compounds with K<sub>d</sub> values of 124 and 137 nM, respectively.

These potent BRD4(1) inhibitors were also evaluated for their cellular antiproliferation activities (Table 5). We selected

**Table 2. Structure–Activity Relationship of the Sulfonamide Derivatives of Benzo[cd]indol-2(1H)-one with Flexible Substituents**

No.	R <sub>1</sub>	R <sub>2</sub>	AlphaScreen ( $\mu\text{M}$ ) <sup>a</sup>	TSA $\Delta T_m$ (°C) <sup>b</sup>	cLogP <sup>c</sup>	LE <sup>d</sup>	No.	R <sub>1</sub>	R <sub>2</sub>	AlphaScreen ( $\mu\text{M}$ ) <sup>a</sup>	TSA $\Delta T_m$ (°C) <sup>b</sup>	cLogP <sup>c</sup>	LE <sup>d</sup>
<b>18</b>	—	Et	>30	1.0	1.43	0.32	<b>37</b>		Et	1.69±0.24	5.5	2.98	0.26
<b>19</b>	—	Et	1.09±0.25	6.1	1.96	0.40	<b>38</b>		Et	1.12±0.19	6.1	3.83	0.27
<b>20</b>	—	Et	0.31±0.05	9.0	2.49	0.41	<b>39</b>		Et	4.10±0.88	3.5	3.27	0.25
<b>21</b>	—	Et	0.44±0.04	8.3	3.02	0.39	<b>40</b>		Et	4.84±0.23	3.4	3.56	0.26
<b>22</b>	—	Et	0.60±0.23	8.0	2.89	0.38	<b>41</b>		Et	5.90±0.14	4.0	2.21	0.27
<b>23</b>	—	Et	1.50±0.57	5.5	3.55	0.34	<b>42</b>		Et	3.18±0.46	5.2	0.71	0.27
<b>24</b>	—	Et	>30	3.5	4.08	<0.25	<b>43</b>		Et	>30	2.5	1.82	<0.23
<b>25</b>		Et	1.16±0.12	7.1	2.88	0.27	<b>44</b>		Et	3.44	4.1	2.21	0.27
<b>26</b>		Et	>30	2.4	0.82	<0.25	<b>45</b>		Et	>30	0	3.03	<0.23
<b>27</b>		Et	0.21±0.04	7.0	2.91	0.39	<b>46</b>		Et	>30	1.3	4.61	<0.23
<b>28</b>		Et	0.13±0.03	10.5	3.47	0.39	<b>47</b>		Et	4.17±0.71	5.0	1.10	0.26
<b>29</b>		Et	0.45±0.07	7.0	4.02	0.34	<b>48</b>		H	>30	1.1	2.76	<0.30
<b>30</b>		Et	1.67±0.13	6.1	1.44	0.34	<b>49</b>		H	>30	2.0	3.21	<0.28
<b>31</b>		Et	>30	1.8	1.30	<0.26	<b>50</b>		Me	8.22±0.44	5.0	2.49	0.32
<b>32</b>		Et	1.21±0.21	7.0	1.07	0.33	<b>51</b>		Me	>30	1.0	2.94	<0.26
<b>33</b>		Et	13.9±1.32	3.5	3.35	0.25	<b>52</b>		Pr	21.13±1.36	3.0	3.55	0.28
<b>34</b>		Et	7.55±0.76	3.5	0.09	0.26	<b>53</b>		Pr	5.21±0.34	4.3	3.99	0.28
<b>35</b>		Et	1.94±0.53	5.3	2.23	0.29	<b>54</b>		i-Bu	>30	0	3.95	<0.26
<b>36</b>		Et	2.58±1.62	4.2	2.74	0.28	<b>55</b>		i-Bu	>30	0	4.39	<0.23

<sup>a</sup>The IC<sub>50</sub> was calculated from AlphaScreen assay. The data were expressed as the means ± SD, representing the data from at least three independent experiments. <sup>b</sup>The  $\Delta T_m$  values were calculated from the thermal shift assay. <sup>c</sup>cLogP values were calculated using ChemBiodraw Ultra12.0. <sup>d</sup>Ligand efficiency (LE) = 1.4 (pIC<sub>50</sub>/heavy atoms).

sensitive cell lines such as leukemia MV4;11, HL-60, and human colon cancer HT-29 cells to test the cellular proliferation inhibition effects. Our compounds exhibited reasonable potency against MV4;11 and HL-60 cell lines but were not well correlated with the other cell lines, which indicated that these analogues were more active against leukemia cancers. Most of the tested compounds revealed more than 60% inhibition at 10  $\mu\text{M}$  in the MV4;11 cell line; however, 73 showed only 25% inhibition and its good protein potency did not translate into the cellular assay. Overall, considering the data from the above assays, 28 and 85 have good profiles for further evaluation.

**2.6. Evaluation of Bromodomains Selectivity.** To investigate the selectivity profile, representative compounds

were tested against 12 bromodomain-containing proteins from different subgroups of the human bromodomain family by thermal stability shift assay (Figure 6). Most of the tested compounds showed excellent selectivity for BET bromodomains over other non-BET bromodomain-containing proteins. The heat map showed that all of the inhibitors tested showed better binding affinity to BRD4(1) than to the other non-BET bromodomain-containing proteins. Some compounds displayed different bromodomain activity profiles. Compounds 14, 60, 68, and 73 displayed moderate activities for EP300. Compound 68 also exhibited weak potency for BRD9. Compounds 17 and 67 showed appreciable inhibitory activity against PCAF, with a temperature shifts of 6.4, and 4.7 °C, respectively, which

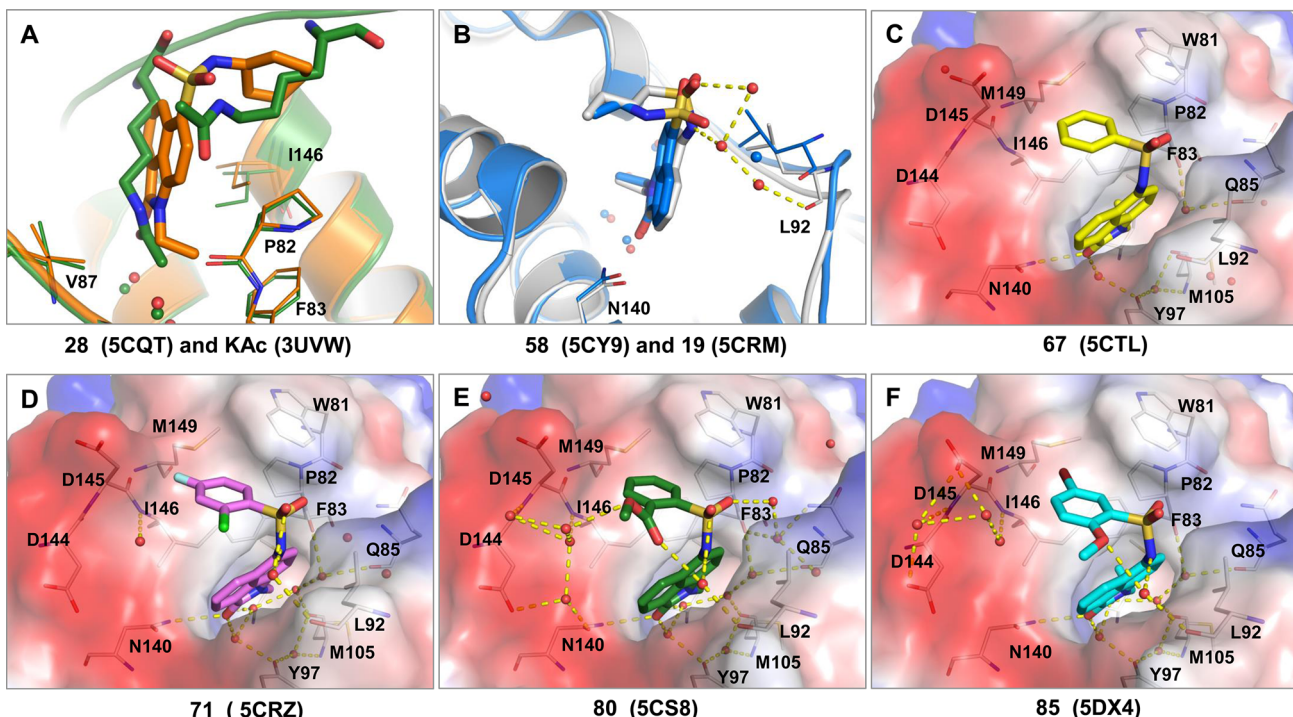


**Figure 5.** (A) Superposition of the crystal structures of **28** and KAc bound to BRD4(1) (PDB IDs: 5CQT and 3UVW). (B) Superposition of the crystal structures of **58** and **19** bound to BRD4(1) (PDB IDs: 5CY9 and 5CRM, respectively). (C–F) Cocrystal structure of compounds **67**, **71**, **80**, and **85** bound to BRD4(1) (PDB IDs: 5CTL, 5CRZ, 5CS8, and 5DX4, respectively). The ligands are shown as sticks models, and the protein is shown as a ribbon model. The electrostatic potential surfaces are also shown. The residues in the binding pocket are shown in lines. Hydrogen bond interactions are indicated by dash lines in yellow. Compounds were well-defined by the electron density. Ligand-omitted electron density maps have been included in the Supporting Information.

indicates that these compounds are promising starting points for developing PCAF inhibitors.

**2.7. Assessment of Pharmacokinetic (PK) Properties and Metabolic Stability for BET Bromodomain Inhibitors **28** and **85**.** To assess the potential of this series of BRD4(1) inhibitors *in vivo*, we conducted preliminary pharmacokinetic analysis for representative sulfonamide and reversed sulfonamide derivatives **28** and **85**. As listed in Table 6, the results showed that **85** had favorable pharmacokinetic properties, whereas **28** displayed unfavorable pharmacokinetic properties in rats. Compound **28** in the oral administration mode demonstrated poor drug exposure with an AUC value of  $85.6 \pm 39.9 \mu\text{g}/\text{L}\cdot\text{h}$  and resulted in lower oral bioavailability (1.7%). In contrast to **28**, the reversed sulfonamide derivative **85** exhibited excellent oral bioavailability (76.8%) and good oral half-life (3.95 h). The results suggest that **85** may have good *in vivo* efficacy when it is orally administered. These two leads were further evaluated for their *in vitro* metabolic stability with rat liver microsome (Table 7). The results showed that **28** was not very stable in the rat liver microsome, as shown by  $T_{1/2}$  of 4.3 and 34.3 min at 1 and 10  $\mu\text{M}$ , respectively. However, **85** exhibited encouraging level of microsomal stability with a  $T_{1/2}$  of 32 min and more than 40 min at 1 and 10  $\mu\text{M}$ , respectively (Table 7). These two compounds were also tested in a Caco-2 monolayer assay to evaluate their cellular permeability (Table 8). Both **28** and **85** showed good cellular permeability with apparent permeability coefficients ( $P_{app}$ ) over  $10 \times 10^{-6} \text{ cm s}^{-1}$  and high recovery values from both directions. The efflux ratio of **28** and **85** were 1.3 and 2.4, respectively, which indicates that these two compounds are not a favorable substrate for P-glycoprotein or any active transport system that might

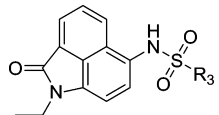
transport it out of the cells. From above data, we conclude that poor oral bioavailability of compound **28** may come from its poor metabolic stability but not cell permeability. Overall, compound **85** exhibited favorable PK properties, cell permeability, and metabolic stability.

### 3. CONCLUSIONS

In this study, we report the discovery of the benzo[*cd*]indol-2(1*H*)-one scaffold as a new class of BET bromodomain inhibitors starting from structure-based virtual screening approach, in conjunction with medicinal chemistry optimization and biological evaluation. Determination of the high-resolution crystal structures provided guidance for extensive structure optimization and resulted in high-potency BET inhibitors. The most promising compound **85** had an  $\text{IC}_{50}$  of 410 nM in the AlphaScreen assay and a  $K_d$  value of 137 nM in the ITC assay. The compound also exhibited reasonable inhibitory activity in the MV4;11 acute leukemia cell line. The excellent bioavailability, cellular permeability, and half-life time make compound **85** a good starting point for further optimization. In summary, these data indicate that the promising compound **85** represents a new class of BET bromodomain inhibitors. Optimization of this series may ultimately lead to a new class of BET inhibitors for treating diseases such as cancers.

### 4. EXPERIMENTAL SECTION

**4.1. Computational Methods.** In the molecular docking study, the crystal structure of BRD4(1) in complex with the inhibitor **1** (PDB ID: 3MXF) was used as the reference structure. Protein structure preparation for docking studies includes water deletion, hydrogen

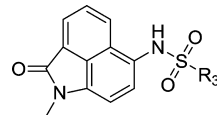
**Table 3. Structure–Activity Relationship of the Reversed Sulfonamide Derivatives of Benzo[cd]indol-2(1H)-one with Flexible Substituents**

No.	R <sub>3</sub>	AlphaScreen ( $\mu\text{M}$ ) <sup>a</sup>	TSA $\Delta T_m$ (°C) <sup>b</sup>	cLogP <sup>c</sup>	LE <sup>d</sup>
56	H	4.27±0.47	5.5	1.78	0.36
57	H	1.17±0.28	7.0	2.31	0.38
58	Et	0.73±0.16	8.9	2.84	0.37
59	iPr	0.46±0.04	8.1	2.62	0.39
60	iBu	0.21±0.05	10.1	3.28	0.37
61	Ph	4.29±0.19	6.0	3.08	0.28
62	4-FPh	5.29±0.33	3.9	3.08	0.27
63	3-FPh	4.9±0.26	5.0	3.08	0.28
64	4-ClPh	4.81±0.21	3.6	3.65	0.28
65	Ph	5.64±0.12	4.5	3.44	0.27

<sup>a</sup>The IC<sub>50</sub> was calculated from the AlphaSceen assay. The data were expressed as the means ± SD, representing the data from at least three independent experiments. <sup>b</sup>The  $\Delta T_m$  values were calculated from the thermal shift assay. <sup>c</sup>cLogP values were calculated using ChemBiodraw Ultra12.0. <sup>d</sup>Ligand efficiency (LE) = 1.4 (pIC<sub>50</sub>/heavy atoms).

atom addition, and protonation state adjustment. All of the ligand and protein preparation were performed in Maestro (version 9.4, Schrödinger, LLC, New York, NY, 2013) implemented in the Schrödinger program (<http://www.schrodinger.com>). Our in-house chemical library with approximately 10000 compounds was selected for structure-based virtual screening. This collection includes compounds with diverse structures from SPECS, ChemDiv, Lifechemicals, and ChemBridge. In this study, molecular docking study was performed with the Glide program (version 6.1, Schrödinger, LLC, New York, NY, 2013) using the SP score mode. Using hydrogen bond constraints with Asn140, 220 structures were selected based on the Glide SP docking score. These 220 structures were further assessed with MMGBSA evaluation, cluster analysis, and visual inspection. At last, 15 representative compounds were kept according to their predicted binding mode, docking score (lower than -6.5 kcal/mol), and binding free energy score (lower than -60 kcal/mol). Finally, selected compounds were submitted for subsequent biological evaluation.

Molecular dynamics (MD) simulations were conducted by using AMBER 14 program. The starting coordinates were obtained from docking results. For ligand coordinates, predicted binding mode of 8-BRD4(1) was used. For protein coordinates, the protein preparation panel in Schrodinger 2014 Suite was applied to assign the protonation states and orientations of residues, which was then further processed by using LEAP module in Amber program. Parameters of compounds were prepared by AM1-bcc model and the other parameters were assigned from the AMBER GAFF force field using ANTECHAMBER. Topology and parameter files for the protein, ligand, and complex were generated using the LEAP module in AMBER 14. TIP3PBOX

**Table 4. Structure–Activity Relationship of the Reversed Phenyl Sulfonamide Derivatives of Benzo[cd]indol-2(1H)-one**

No.	R <sub>3</sub>	AlphaScreen ( $\mu\text{M}$ ) <sup>a</sup>	TSA $\Delta T_m$ (°C) <sup>b</sup>	cLogP <sup>c</sup>	LE <sup>d</sup>
66	Ph	1.19±0.14	7.5	2.65	0.35
67	Ph	0.30±0.05	10.2	2.88	0.37
68	4-FPh	0.40±0.11	9.5	3.15	0.34
69	3-FPh	0.62±0.09	8.0	3.15	0.33
70	4-BrPh	0.51±0.08	7.2	3.37	0.34
71	3-ClPh	0.45±0.04	7.1	3.61	0.33
72	3-FPh	1.72±0.38	7.1	3.91	0.30
73	4-FPh	0.12±0.03	9.5	3.34	0.36
74	3,5-Cl <sub>2</sub> Ph	5.56±0.17	3.1	3.88	0.27
75	3,4-Cl <sub>2</sub> Ph	2.55±0.27	4.5	4.06	0.29
76	3,5-Cl <sub>2</sub> Ph	>30	2.4	4.48	<0.23
77	Ph	0.53±0.20	9.0	3.38	0.34
78	Ph-CN	2.98±0.11	6.1	2.84	0.29
79	Ph-NO <sub>2</sub>	2.28±0.06	6.5	3.09	0.28
80	Ph-O <sup>-</sup>	2.29±0.11	6.0	2.52	0.27
81	Ph-OH	1.58±0.08	6.0	2.91	0.29
82	Ph-O <sup>2-</sup>	3.13±0.03	5.1	3.22	0.27
83	Ph-OH	3.51±0.34	5.7	2.91	0.27
84	3-ClPh	0.47±0.06	8.5	3.37	0.32
85	3-BrPh	0.41±0.03	9.9	3.52	0.32
86	Ph-O <sup>-</sup>	3.87±0.36	5.0	2.57	0.26

<sup>a</sup>The IC<sub>50</sub> was calculated from theAlphaScreen assay. The data were expressed as the means ± SD, representing the data from at least three independent experiments. <sup>b</sup>The  $\Delta T_m$  values were calculated from the thermal shift assay. <sup>c</sup>cLogP values were calculated using ChemBiodraw Ultra12.0. <sup>d</sup>Ligand efficiency (LE) = 1.4 (pIC<sub>50</sub>/heavy atoms).

water molecules were added in cube periodic boxes, which were 10 Å × 10 Å × 10 Å. To ensure overall neutrality of the system, appropriate Na<sup>+</sup> and Cl<sup>-</sup> were added at physiological concentration in the box. For each system, energy minimization and MD simulation were carried out using the GPU version of the PMEMD program in AMBER 14 program. The MD simulations were performed for up to 20 ns for each complex system. The coordinates of the complexes were saved every 2 ps, whose snapshots were taken in production run for detailed analysis. Trajectories were analyzed using the PTraj module in Amber 14.

**Table 5. Isothermal Titration Calorimetric Study of the Binding Affinity of Selected Potent Inhibitors with BRD4(1) and Antiproliferation Effects against Cell Lines MV4;11, HL-60, and HT-29<sup>a</sup>**

no.	$K_d$ ( $\mu\text{M}$ )	$\Delta H$ (kcal)	MV4;11 IC <sub>50</sub> ( $\mu\text{M}$ ) <sup>b</sup>	HL-60 IC <sub>50</sub> ( $\mu\text{M}$ )	HT-29 IC <sub>50</sub> ( $\mu\text{M}$ )
1	0.034	-10.8	0.012 ± 0.005	0.06	0.28
14	0.392	-12.3	NA	NA	NA
17	1.234	-9.4	11.93 ± 1.32	NA	38.3
20	0.224	-11.5	1.32 ± 0.17	2.95	14.6
25	0.421	-13.7	5.48 ± 0.86	43.1	48.1
28	0.124	-11.6	3.46 ± 0.80	2.01	8.50
42	2.340	-10.2	8.75 ± 0.90	17.9	46.8
47	3.751	-7.5	9.54 ± 1.12	28.3	49.0
58	0.218	-16.0	4.71 ± 0.30	4.16	NA
60	0.255	-19.2	2.85 ± 0.50	3.86	8.10
68	0.390	-14.0	3.09 ± 0.42	NT	NT
73	0.275	-13.2	4.19 ± 0.16	NT	NT
84	0.180	-14.5	2.84 ± 0.86	3.00	8.20
85	0.137	-15.8	1.30 ± 0.23	2.99	12.9

<sup>a</sup> $K_d$  and  $\Delta H$  were determined from the isothermal titration calorimetric assay. The IC<sub>50</sub> values were calculated from cell viability assay. NA = no activity. NT = not tested. <sup>b</sup>The data were expressed as the means ± SD, representing the relative levels of antiproliferation from at least three independent experiments.

**4.2. General Chemistry.** Synthesis of the desired reagents and solvents were obtained from commercial suppliers and used without further purification. Flash chromatography was performed using silica gel (300–400 mesh). All reactions were monitored by TLC, using silica gel plates with fluorescence F254 and UV light visualization. <sup>1</sup>H NMR spectra were recorded on a Bruker AV-400 spectrometer at 400 MHz and <sup>13</sup>C NMR spectra were recorded on a Bruker AV-500 spectrometer at 500 MHz. Coupling constants ( $J$ ) are expressed in hertz (Hz). Chemical shifts ( $\delta$ ) of NMR are reported in parts per million (ppm) units relative to internal control (TMS). The low-resolution of ESI-MS was recorded on an Agilent 1200 HPLC-MSD mass spectrometer. The purity of compounds was determined to be over 95% by reverse-phase high performance liquid chromatography (HPLC) analysis. HPLC instrument: Dionex Summit HPLC (column: Inertsil ODS-SP, 5.0  $\mu\text{m}$ , 4.6 mm × 250 mm (GL Sciences Inc.);

detector, UVD170U; injector, manual injector; pump, P680; detection wavelength, 254 nm; flow rate, 1.0 mL/min.

**4.2.1. Procedure 1a of Scheme 1.** Benzo[*de*]isochromene-1,3-dione (87) (6 g, 30 mmol) and hydroxylamine hydrochloride (2 g, 30 mmol) were combined as a solution in pyridine (40 mL). The reaction was conducted under reflux for 1 h followed by cooling to 80 °C. To the reaction system mixture was added powdered *p*-toluenesulfonyl chloride (11.5 g, 60 mmol). After the addition, the reaction was performed under reflux for 1 h. After cooling to room temperature, the reaction mixture was poured into ice water (300 mL) and stirred to precipitate crystals. The precipitate was filtered and rinsed with additional cool water (100 mL) and saturated NaHCO<sub>3</sub> (100 mL) to give 1,3-dioxo-1*H*-benzo[*de*]isoquinolin-2(3*H*)-yl 4-methylbenzenesulfonate (88) (8.6 g, 78%) as a yellow solid.

**4.2.2. Procedure 1b of Scheme 1.** To a solution of 88 (8.6 g, 23.5 mmol) in ethanol (50 mL) and water (40 mL) was added an aqueous solution of sodium hydroxide (2.7 mol/L, 30 mL) at room temperature. The mixture was heated to reflux temperature for 3 h while distilling the ethanol. After the reaction was completed, the reaction mixture was cooled to 75 °C, concentrated hydrochloric acid was added dropwise, and a yellow precipitate was formed. Then, the mixture was further cooled. The precipitate was collected by filtration and washed with water (100 mL × 2). The resulting crude product was purified by silica gel chromatography with dichloromethane to give benzo[cd]indol-2(1*H*)-one (89) (3.3 g, 83%) as a yellow solid. <sup>1</sup>H NMR (400 MHz, DMSO)  $\delta$  10.75 (s, 1H), 8.16 (d,  $J$  = 8.0 Hz, 1H), 8.01 (d,  $J$  = 6.8 Hz, 1H), 7.78 (t,  $J$  = 7.6 Hz, 1H), 7.65 (d,  $J$  = 8.4 Hz, 1H), 7.48 (t,  $J$  = 7.2 Hz, 1H), 6.98 (d,  $J$  = 7.2 Hz, 1H).

**4.2.3. Procedure 1c of Scheme 1.** The product 89 (3.3 g, 20 mmol) and potassium carbonate (5.4 g, 39 mmol) were dissolved in DMF (50 mL). Ethyl iodide (3.65 g, 23.5 mmol) was added dropwise. The reaction mixture was stirred at 50 °C overnight. The reaction mixture was extracted with ethyl acetate (150 mL × 2). The organic layer was washed with brine and dried over Na<sub>2</sub>SO<sub>4</sub>. The solid was filtered off, and the filtrate was concentrated under reduced pressure. The resulting crude product was purified by silica gel chromatography with petroleum ether/ethyl acetate (10/1, v/v) to yield 1-ethylbenzo[cd]indol-2(1*H*)-one (90a) (3.1 g, 78%) as a yellow oil. MS (APCI), *m/z* for C<sub>13</sub>H<sub>11</sub>NO ([M + H]<sup>+</sup>): calcd, 197.24; found, 198.0.

**4.2.4. Procedure 1d of Scheme 1.** To a solution of 90a (3.23 g, 16.5 mmol) in chloroform (100 mL) was added batches of chlorosulfonic (5.8 g, 50 mmol) at 0 °C for 10 min. The reaction mixture was heated at 50 °C for 6 h. The mixture was then poured into ice water and extracted with DCM (150 mL × 2). The organic layer



**Figure 6.** Benzo[cd]indol-2(1*H*)-one derivatives are selective BET inhibitors. The bromodomains selectivity profiles were determined by thermal shift assay. **1**, *N*-[(6-3-methanesulfonamido-4-methylphenyl)-3-methyl-1,2,4-triazolo[4,3-*b*]pyridazin-8-yl]carbamate (bromosporine) and 2-[2-(3-chloro-4-methoxyphenyl)ethyl]-5-(dimethyl-1,2-oxazol-4-yl)-1-[(2S)-2-(morpholin-4-yl)propyl]-1*H*-1,3-benzodiazole (SGC-CBP30)<sup>19</sup> were used as positive control. Compound concentration, 200  $\mu\text{M}$ ; protein concentration, 10  $\mu\text{M}$ . Heat map shows the relative  $\Delta T_m$  values. Red indicates large  $\Delta T_m$ , and green indicates small  $\Delta T_m$ .

**Table 6.** Intravenous (iv) and Oral (po) Pharmacokinetic Profiles of Compounds 28 and 85 in Rats<sup>a</sup>

route	$C_{\max}$ ( $\mu\text{g}/\text{L}$ )	$T_{\max}$ (h)	$AUC_{0-t}$ ( $\mu\text{g}/\text{L}\cdot\text{h}$ )	$AUC_{0-\infty}$ ( $\mu\text{g}/\text{L}\cdot\text{h}$ )	$T_{1/2}$ (h)	$CL_z/F$ ( $\text{L}/\text{h}/\text{kg}$ )	$V_z/F$ ( $\text{L}/\text{kg}$ )	$F$ (%)
28 iv (5 mg/kg)	875 ± 14.2	0.033 ± 0	812 ± 7.2	818 ± 7.3	1.13 ± 0.02	6.12 ± 0.06	9.98 ± 0.15	
28 po (30 mg/kg)	37.3 ± 24.1	0.42 ± 0.29	80.3 ± 46.5	85.6 ± 39.9	1.74 ± 1.11			1.7
85 iv (5 mg/kg)	2172 ± 702.8	0.033 ± 0	716.5 ± 246.6	718.6 ± 248.0	0.98 ± 0.28	7.94 ± 3.42	10.1 ± 1.3	
85 po (20 mg/kg)	516.2 ± 58.9	0.42 ± 0.26	2202 ± 331.9	2214 ± 338.0	3.95 ± 1.37			76.8

<sup>a</sup>The pharmacokinetic parameters were tested in 6 rats. Compounds were formulated in 2% DMSO, 5% EtOH, 3% Tween80, and 90% H<sub>2</sub>O.

**Table 7.** Metabolic Stability of 28 and 85 in Rat Liver Microsomes

compd	microsomal stability (%parent @ 40 min)		$T_{1/2}$ (min)	
	1 $\mu\text{M}$ (%)	10 $\mu\text{M}$ (%)	1 $\mu\text{M}$	10 $\mu\text{M}$
28	4.5	57.5	4.3	34.3
85	57.2	>85	32.4	>40.0

was washed with brine and dried over Na<sub>2</sub>SO<sub>4</sub>. The solid was filtered off, and the filtrate was concentrated under reduced pressure. The resulting crude product was purified by silica gel chromatography with petroleum ether/ethyl acetate (5/1, v/v) to yield 1-ethyl-2-oxo-1,2-dihydrobenzo[cd]indole-6-sulfonyl chloride (91a) (2.9 g, 59%) as a yellow solid. <sup>1</sup>H NMR (400 MHz, DMSO)  $\delta$  8.72 (d,  $J$  = 8.0 Hz, 1H), 8.00 (d,  $J$  = 6.8 Hz, 1H), 7.84 (t,  $J$  = 7.2 Hz, 1H), 7.78 (d,  $J$  = 7.6 Hz, 1H), 3.89 (q,  $J$  = 6.8 Hz, 2H), 1.24 (t,  $J$  = 7.2 Hz, 3H).

**4.2.5. Procedure 1e of Scheme 1.** A reaction mixture of compound 91a (70 mg, 0.237 mmol) and propan-1-amine (17 mg, 0.284 mmol) in pyridine (4 mL) was stirred at 80 °C for 1 h. Dilute HCl was added, the aqueous layer was extracted with ethyl acetate (50 mL × 3), and the organic layer was washed with water and brine, dried with Na<sub>2</sub>SO<sub>4</sub>, and evaporated. The residue was purified by silica gel chromatography with petroleum and ether/ethyl acetate (4/1, v/v) to afford 1-ethyl-2-oxo-N-propyl-1,2-dihydrobenzo[cd]indole-6-sulfonamide (20) (54 mg, 71%). <sup>1</sup>H NMR (400 MHz, CDCl<sub>3</sub>)  $\delta$  8.65 (d,  $J$  = 8.4 Hz, 1H), 8.18 (d,  $J$  = 7.6 Hz, 1H), 8.10 (d,  $J$  = 7.2 Hz, 1H), 7.92–7.68 (m, 1H), 6.92 (d,  $J$  = 7.6 Hz, 1H), 4.66 (t,  $J$  = 6.0 Hz, 1H), 3.98 (q,  $J$  = 7.2 Hz, 2H), 2.91 (dd,  $J$  = 13.2, 6.8 Hz, 2H), 1.46 (dt,  $J$  = 14.4, 7.2 Hz, 2H), 1.39 (t,  $J$  = 7.2 Hz, 3H), 0.80 (t,  $J$  = 7.2 Hz, 3H). <sup>13</sup>C NMR (500 MHz, CDCl<sub>3</sub>)  $\delta$  167.7, 143.9, 132.9, 130.6, 129.5, 128.7, 126.9, 126.1, 125.4, 124.9, 103.0, 45.0, 35.2, 23.0, 14.0, 11.1. MS (APCI),  $m/z$  for C<sub>16</sub>H<sub>18</sub>N<sub>2</sub>O<sub>3</sub>S ([M – H]<sup>-</sup>): calcd, 318.39; found, 317.0. HPLC analysis: MeOH – H<sub>2</sub>O (80:20), 4.52 min, 99.78% purity.

The synthesis of 9–13, 17–19, 21–26, and 33, 37–47 can refer to 20 (for details, see Supporting Information).

**4.2.6. Another Procedure 1e of Scheme 1.** To a reaction mixture of compound 91a (70 mg, 0.237 mmol) and cyclohexanamine (28 mg, 0.284 mmol) in DCM (10 mL) was added DIPEA (0.5 mL), and the reaction mixture stirred at room temperature for 3 h. Added water, extracted with DCM (50 mL × 3), and the organic layer was washed with water and brine, dried with Na<sub>2</sub>SO<sub>4</sub>, and evaporated. The residue was purified by silica gel chromatography with petroleum and ether/ethyl acetate (3/1, v/v) to afford N-cyclohexyl-1-ethyl-2-oxo-1,2-dihydrobenzo[cd]indole-6-sulfonamide (28) (76 mg, 89%) as a yellow solid. <sup>1</sup>H NMR (400 MHz, CDCl<sub>3</sub>)  $\delta$  8.61 (d,  $J$  = 8.4 Hz, 1H), 8.20 (d,

$J$  = 7.6 Hz, 1H), 8.11 (d,  $J$  = 7.2 Hz, 1H), 7.84 (t,  $J$  = 7.2 Hz, 1H), 6.92 (d,  $J$  = 7.6 Hz, 1H), 4.52 (d,  $J$  = 7.6 Hz, 1H), 3.99 (q,  $J$  = 7.2 Hz, 2H), 3.29–2.92 (m, 1H), 1.75–1.63 (m, 2H), 1.58–1.50 (m, 1H), 1.49–1.46 (m, 1H), 1.40 (t,  $J$  = 7.2 Hz, 3H), 1.25–1.05 (m, 6H). <sup>13</sup>C NMR (500 MHz, CDCl<sub>3</sub>)  $\delta$  168.0, 144.0, 132.8, 130.7, 130.2, 129.7, 127.1, 126.3, 125.5, 125.0, 103.2, 125.9, 53.0, 35.4, 34.3, 25.4, 24.9, 14.2. MS (APCI),  $m/z$  for C<sub>19</sub>H<sub>22</sub>N<sub>2</sub>O<sub>3</sub>S ([M + H]<sup>+</sup>): calcd, 358.46; found, 359.1. HPLC analysis: MeOH – H<sub>2</sub>O (80:20), 5.67 min, 99.20% purity.

The synthesis of 27, 29–30, 32, 34–35, and 48–55 can refer to 28 (for details, see Supporting Information).

**4.2.7. Procedure 2a of Scheme 2.** To a solution of 1-ethylbenzo[cd]indol-2(1H)-one (90a) (2 g, 10.1 mmol) in AcOH (20 mL) was added HNO<sub>3</sub> (0.64 g, 10.1 mmol) at 0 °C and then the reaction mixture was stirred at 50 °C for 1 h. After the reaction was completed, the reaction mixture was cooled to rt. The reaction mixture was extracted with ethyl acetate (150 mL × 2). The organic layer was washed with brine and dried over Na<sub>2</sub>SO<sub>4</sub>. The solid was filtered off, and the filtrate was concentrated under reduced pressure. The resulting crude product was purified by silica gel chromatography with petroleum ether/ethyl acetate (6/1, v/v) to yield 1-ethyl-6-nitrobenzo[cd]indol-2(1H)-one (92) (1.8 g, 73%) as a yellow solid. MS (APCI),  $m/z$  for C<sub>13</sub>H<sub>10</sub>N<sub>2</sub>O<sub>3</sub> ([M + H]<sup>+</sup>): calcd, 242.23; found, 243.1.

**4.2.8. Procedure 2b of Scheme 2.** A reaction mixture of Fe power (2.1 g, 37 mmol) and NH<sub>4</sub>Cl (0.8 g, 14.9 mmol) in AcOH (20 mL) and water (80 mL) was heated at 50 °C for 5 min. 1-Ethyl-6-nitrobenzo[cd]indol-2(1H)-one (1.8 g, 7.43 mmol) was dissolved in DMF (15 mL) and added to the reaction mixture. After the reaction was completed, and the reaction mixture was cooled to rt. The reaction mixture was extracted with ethyl acetate (150 mL × 2). The organic layer was washed with brine and dried over Na<sub>2</sub>SO<sub>4</sub>. The solid was filtered off, and the filtrate was concentrated under reduced pressure. The resulting crude product was purified by silica gel chromatography with petroleum ether/ethyl acetate (3/1, v/v) to yield 6-amino-1-ethylbenzo[cd]indol-2(1H)-one (93) (1.38 g, 87.5%) as a yellow solid. <sup>1</sup>H NMR (400 MHz, CDCl<sub>3</sub>)  $\delta$  8.06 (d,  $J$  = 7.2 Hz, 1H), 8.00 (d,  $J$  = 8.4 Hz, 1H), 7.67 (t,  $J$  = 7.6 Hz, 1H), 6.73 (d,  $J$  = 7.6 Hz, 1H), 6.63 (d,  $J$  = 7.6 Hz, 1H), 4.10 (s, 2H), 3.95 (q,  $J$  = 7.2 Hz, 2H), 3.95 (t,  $J$  = 7.2 Hz, 3H).

**4.2.9. Procedure 2c of Scheme 2.** To a solution of compound 93 (70 mg, 0.33 mmol) and cyclohexanesulfonyl chloride (66 mg, 0.36 mmol) in DCM (4 mL) was added pyridine (0.5 mL). The mixture was stirred at rt for 2 h. The reaction mixture was extracted with DCM (50 mL × 2). The organic layer was washed with brine and dried over Na<sub>2</sub>SO<sub>4</sub>. The solid was filtered off, and the filtrate was concentrated under reduced pressure. The resulting crude product was purified by silica gel chromatography with petroleum ether/ethyl acetate (2/1, v/v)

**Table 8.** Caco-2 Permeability Summary for 28 and 85<sup>a</sup>

compd	apparent permeability ( $P_{app}$ , $10^{-6}$ cm s <sup>-1</sup> ) <sup>b</sup>		efflux ratio <sup>c</sup>	recovery (%)	
	mean A→B	mean B→A		A→B	B→A
28	21.2 ± 2.7	28.0 ± 3.1	1.3 ± 0.1	90.0 ± 5.4	85.0 ± 1.7
85	12.7 ± 0.5	30.9 ± 1.4	2.4 ± 0.2	110.7 ± 2.3	116.8 ± 2.8
digoxin <sup>d</sup>	1.6 ± 0.0	17.7 ± 0.2	11.2 ± 0.2	107.0 ± 6.4	111.0 ± 7.8

<sup>a</sup>All assays were performed over 1 h at a concentration of 10  $\mu\text{M}$ . “A to B” indicates the experiment from apical to basolateral, and “B to A” indicates the experiment from basolateral to apical. <sup>b</sup> $P_{app}$ : apparent permeability rate coefficient. <sup>c</sup>Efflux ratio:  $P_{app}$  (B→A)/ $P_{app}$  (A→B). <sup>d</sup>Digoxin was used as positive control.

v) to yield *N*-(1-ethyl-2-oxo-1,2-dihydrobenzo[*cd*]indol-6-yl)-cyclohexanesulfonamide (**60**) (80 mg, 67%) as a yellow solid. <sup>1</sup>H NMR (400 MHz, CDCl<sub>3</sub>) δ 8.23 (d, *J* = 8.4 Hz, 1H), 8.09 (d, *J* = 7.2 Hz, 1H), 7.78 (t, *J* = 7.6 Hz, 1H), 7.55 (d, *J* = 7.6 Hz, 1H), 7.00–6.72 (m, 2H), 3.96 (q, *J* = 7.2 Hz, 2H), 3.21–2.96 (m, 1H), 2.23 (d, *J* = 11.2 Hz, 2H), 1.87 (d, *J* = 7.6 Hz, 2H), 1.65–1.61 (m, 4H), 1.37 (t, *J* = 7.2 Hz, 3H), 1.19 (d, *J* = 9.2 Hz, 2H). <sup>13</sup>C NMR (500 MHz, CDCl<sub>3</sub>) δ 167.8, 138.2, 129.6, 127.5, 127.4, 126.7, 126.1, 125.2, 124.3, 124.2, 105.2, 61.0, 35.3, 26.9, 25.4, 25.3, 14.3. MS (ESI), *m/z* for C<sub>19</sub>H<sub>22</sub>N<sub>2</sub>O<sub>3</sub>S ([M + H]<sup>+</sup>): calcd, 358.46; found, 359.0. HPLC analysis: MeOH – H<sub>2</sub>O (80:20), 5.17 min, 99.02% purity.

The synthesis of **56–59**, **61–80**, **82**, and **84–86** can refer to **60** (for details, see Supporting Information).

**4.3. Biological Evaluation.** **4.3.1. Protein Expression and Purification.** The bromodomains were expressed as a His6-fusion protein with a TEV cleavage site between His6 and bromodomain using the pET24a expression vector (Novagen). cDNA encoding bromodomain of human BRD2(1) (residues K77-N194), BRD3(1) (residues P24-E144), BRD4(1) (residues N44-E168), BRDT(1) (residues N21-E137), EP300 (residues A1040-G1161), CREBBP (residues R1081-G1197), BRD1 (residues E556-A688), BRD9 (residues L14-Q134), PCAF (residues G715-D831), ASHIL (residues E2433-E2564), BAZ2B (residues S1858-S1972), and TAF1(1) (residues R1377-D1503) were synthesized by Genscript. BL21 (DE3) cells transformed with these expression plasmids were grown in LB broth at 25 °C to an OD<sub>600</sub> of approximately 1.0 and then induced with 0.1 mM isopropyl-β-D-1-thiogalactopyranoside (IPTG) at 16 °C for 16 h. Cells were harvested by centrifugation (6000g for 15 min at 4 °C, JLA 81000 rotor, on a Beckman Coulter Avanti J-20 XP centrifuge) and were frozen at –80 °C as pellets for storage. Cells were resuspended in extract buffer (50 mM HEPES, pH 7.5 at 25 °C, 500 mM NaCl, 5 mM imidazole, 5% glycerol, and 0.5 mM TCEP (Tris(2-carboxyethyl)phosphine hydrochloride)) and high-pressure homogenized using an JN3000 PLUS high pressure homogenizer (JNBIO, Guangzhou, China) at 4 °C. The lysate was collected on ice and centrifuged at 12000g for 40 min. The supernatant was loaded onto a 5 mL NiSO<sub>4</sub>-loaded HisTrap HP column (Ni-NTA, GE Healthcare, NJ). The column was washed with 20 mL of extract buffer (50 mM HEPES, pH 7.5 at 25 °C, 500 mM NaCl, 50 mM imidazole). The protein was eluted with a 50–500 mM imidazole gradient in elute buffer with (50 mM HEPES, pH 7.5 at 25 °C, 500 mM NaCl, 500 mM imidazole). The protein was concentrated and further purified by a gel filtration column (HiLoad, Superdex 75, 16/60, GE Healthcare). The sample purity of each fraction was examined by SDS-PAGE, and the sample concentration was determined by Bradford assay. Purified proteins were concentrated and stored in the gel filtration buffer (10 mM Hepes pH 7.5 at 25 °C, 150 mM NaCl, 0.5 mM TCEP) and were used for crystallization or stored at –80 °C for AlphaScreen, TSA, or ITC assay.

**4.3.2. AlphaScreen Assay.** Interactions between bromodomain-containing proteins (BCP) and ligands were assessed by luminescence-based AlphaScreen technology (PerkinElmer) as previously described in using a histidine detection kit from PerkinElmer (Norwalk, CT). All of the reactions contained bromodomain-containing protein bound to nickel acceptor beads (5 μg/mL) and biotinylated acetylated histone H4 peptide bound to streptavidin donor beads (5 μg/mL) in the presence or absence of the indicated amounts of control compounds **1**, or candidate compounds. The C-terminal biotinylated tetra-acetylated histone peptide H4 (bH4KAc4) sequence was H-SGRGK(Ac)GGK-(Ac)GLGK(Ac)GGAK(Ac)RHRK-Biotin-OH (synthesized by Genscript). The experiments were conducted with various protein/peptide ratio as follows for sensitive signal: BRD4(1):bH4KAc4 = 50 nM, 50 nM; CREBBP:bH4KAc4 = 200 nM, 50 nM; BRD1:H4KAc4 = 100 nM, 50 nM; BRD9:H4KAc4 = 150 nM, 50 nM; BRD2(2):H4KAc4 = 150 nM, 100 nM; BRD3(2):H4KAc4 = 100 nM, 50 nM; BRD4(2):H4KAc4 = 100 nM, 50 nM; ATAD2:H4KAc4 = 100 nM, 100 nM; BAZ2B:H3K14Ac = 150 nM, 100 nM.

All reagents were diluted in the buffer (50 mM MOPS, pH 7.4, 50 mM NaF, 50 μM CHAPS, and 0.1 mg/mL bovine serum albumin) and allowed to equilibrate at room temperature prior to addition to

low-volume 384-well plates (ProxiPlate-384 Plus, PerkinElmer, USA). Plates were foil sealed to protect from light, incubated at room temperature for 2 h, and read on an EnSpire plate reader (PerkinElmer, USA). When excited by a laser beam of 680 nm, the donor beam emits singlet oxygen that activates thioxene derivatives in the acceptor beads, which releases photons of 520–620 nm as the binding signal. All experiments were carried out in triplicate on the same plate. The results were based on an average of three experiments with standard errors typically less than 10% of the measurements.

**4.3.3. Thermal Stability Shift Assay (TSA).** Thermal stability shift assays were carried out using the Bio-Rad CFX96 Real-Time PCR system. All reactions were buffered in 10 mM HEPES, pH 7.5, 150 mM NaCl at a final concentration of 10 μM proteins and 200 μM compounds. The 20 μL reaction mix was added to the wells of 96-well PCR plate. SYPRO Orange (ABI, Sigma) was added as a fluorescence probe at a dilution of 1:1000 and incubated with compounds on ice for 30 min. Total DMSO concentration was restricted to 1% or less. Excitation and emission filters for the SYPRO Orange dye were set to 465 and 590 nm, respectively. The temperature was raised with a step of 0.3 °C per minute from 30 to 75 °C, and fluorescence readings were taken at each (0.3 °C) interval. All experiments were performed in triplicates. Melting temperatures (T<sub>m</sub>) were calculated by fitting the sigmoidal melt curve to the Boltzmann equation using GraphPad Prism. ΔT<sub>m</sub> is the difference in T<sub>m</sub> values calculated for reactions with and without compounds.

**4.3.4. Isothermal Titration Calorimetry (ITC).** The ITC measurements were carried out using an ITC200 instrument (Microcal, GE Healthcare). All experiments were performed at 25 °C while stirring at 1000 rpm in an ITC buffer (50 mM HEPES, 150 mM NaCl, 0.5 mM TCEP and pH 7.5). All titrations of bromodomain-containing proteins into ligands were performed using an initial injection of 0.5 μL followed by 20 identical injections of 2 μL with a duration of 4 s per injection and a spacing of 180 s between injections. The stock solutions of ligands and the bromodomain-containing proteins were diluted with the ITC buffer to a compound concentration of 40–60 μM and protein concentration of 500–600 μM before titrations. The final concentration of DMSO in the reaction buffer is less than 0.25% of the total volume. To estimate the background of the heat of dilution for the proteins, the proteins were titrated into ITC buffer on separate experiments. Data was corrected for heats of dilution by subtracting the data from independent titrations of proteins into buffer. In all the cases, a single binding site mode was employed and a nonlinear least-squares algorithm was used to obtain best-fit values of the stoichiometry (*n*), change in enthalpy (ΔH), and binding constant (K<sub>d</sub>). Thermodynamic parameters were subsequently calculated with the formula ΔG = ΔH – TΔS = –RT ln K, where ΔG, ΔH, ΔS, T, and R are the changes in free energy, enthalpy, entropy of binding, experimental temperature, and the gas constant, respectively. Titrations were run in triplicate to ensure reproducibility. MicroCal Origin7 software was used to collect and process the data.

**4.3.5. Cell Culture and Growth Inhibition Assays.** Cells were seeded in 96-well plates at a concentration of 5 × 10<sup>3</sup> cells per well. Cells were grown in 100 μL of IMDM containing 10% fetal bovine serum. After 24 h, 50 μL of chemical compounds (triple diluted) was added to each well with final concentration from 5 nM to 100 μM. The measurement was conducted 72 h after seeding, and 10 μL of CCK8 kit reagent was added to each well and incubated in 37 °C for 4 h. The absorbance at 450 nm was detected with Epoch multivolume spectrophotometer system (Bioteck). The inhibition rate was calculated as [(A<sub>450</sub> treated – A<sub>450</sub> blank)/(A<sub>450</sub> control – A<sub>450</sub> blank)] × 100. Inhibition curve was fitted with Graphpad (prism), and GI<sub>50</sub> was obtained.

**4.3.6. Crystallization, Data Collection, and Structure Determination.** The purified and concentrated (10–15 mg/mL) BRD4(1) protein was incubated with ligands at a molar ratio of 1:3 for 40 min on ice. All crystallizations were carried out using the sitting drop vapor diffusion method in 24-well plate at 4 °C. Crystals of BRD4(1) with ligands were grown by mixing 1 μL of the protein (8–15 mg/mL) with 1 μL of reservoir solution containing various well buffers. Crystals of BRD4(1) with **17** were grown with reservoir solution containing 0.2

M ( $\text{NH}_4$ )<sub>2</sub>SO<sub>4</sub>, 0.1 M HEPES, pH 7.5, 20% PEG3350, and 10% ethylene glycol. Crystals of BRD4(1) with **19**, **28**, **29**, **36**, **42**, **67**, **71**, **80**, and **85** were grown with reservoir solution containing 0.2 M NaNO<sub>3</sub>, 0.1 M HEPES, pH 6.5–8.0, 20% PEG3350, and 10% ethylene glycol. Crystals of BRD4(1) with **58** were grown with reservoir solution containing 0.2 M NaCl, 0.1 M HEPES, pH 7.8, 20% PEG3350, and 10% ethylene glycol.

Most crystals appeared in 2 days and grew to full size approximately 1 week. Crystals were cryoprotected using the well solution supplemented with additional ethylene glycol and were flash frozen in liquid nitrogen. All diffraction data were collected on beamlines BL17U and BL19U1 at Shanghai Synchrotron Radiation Facilities (SSRF) at 100 K. Data sets were processed (indexing and integration) using the program MOSFLM<sup>36</sup> and scaled using Aimless from the Collaborative Computational Project 4 (CCP4) program suite.<sup>37</sup> Molecular replacement was performed with the CCP4 program Phaser<sup>38</sup> using 1–BRD4(1) complex structure (PDB ID: 3MXF) as a search model. The model was refined using CCP4 program REFMAC5<sup>39</sup> and rebuilt with COOT.<sup>40</sup> The quality of the models was checked using MolProbity.<sup>41</sup> Structure figures were prepared using the program PyMOL.<sup>42</sup> The statistics of data collection and the model refinement are summarized in Supporting Information, Table S2. Crystals of **17**, **19**, **28**, **29**, **36**, **42**, **58**, **67**, **71**, **80**, and **85** with BRD4(1) diffracted to resolutions of 1.79, 1.99, 1.60, 1.62, 1.49, 1.55, 2.12, 1.49, 1.62, 2.51, and 2.30 Å, respectively.

**4.3.7. Pharmacokinetics Analysis.** Pharmacokinetic properties of **28** and **85** were analyzed by Zhongshan Pharmass Corporation, Guangzhou, China. Fifteen Sprague–Dawley rats (200–220 g) were provided by Guangdong Medical Laboratory Animal Center. They were fasted overnight and allowed free access to water before administration. All procedures involving animals were in accordance with the Regulations of Experiment Animal Administration issued by the State Committee of Science and Technology of China. **28** was dissolved with distilled water:ethanol (95:5, v/v) as stock solution (4 mg/mL). The stock solution was orally administrated to 6 SD rats at the dose of 30 mg/kg and intravenous administrated to 6 SD rats at a single dose of 5 mg/kg. **85** was dissolved with distilled water:ethanol (95:5, v/v) as stock solution (4 mg/mL). The stock solution was orally administrated to 6 SD rats at the dose of 25 mg/kg and intravenous administrated to 6 SD rats at a single dose of 5 mg/kg. Blood was collected from the suborbital vein before administration and at 0.083, 0.25, 0.75, 1.5, 3, 5, 7, 9, 12, 15, and 24 h after dosing for oral group. Blood was collected from the suborbital vein before administration and at 0.033, 0.17, 0.5, 1, 2, 3, 4, 6, 8, 12, and 24 h after dosing for intravenous group. About 300 μL blood samples were collected into heparinized tubes and then immediately centrifuged at 4000g for 10 min. The plasma obtained was stored at –20 °C until analysis.

**4.3.8. Microsomal Stability Assay.** This assay was performed by Zhongshan Pharmass Corporation, Guangzhou, China. First, 1 μM and 10 μM compounds were incubated with 0.5 mg/mL rat liver microsomes (RLM was purchased from Research Institute for Liver Diseases (Shanghai) Co. Ltd.). NADPH was maintained at 1 mM in 1000 μL reaction volume. The reaction was then evaluated at 0, 3, 6, 10, 20, and 40 min and was terminated by the addition of acetonitrile. Samples were centrifuged for 10 min at 12000 rpm and supernatant analyzed using HPLC-MS/MS. Percentage parent remaining was calculated considering percent parent area at 0 min as 100%.

**4.3.9. Caco-2 Permeability Assay.** Caco-2 permeability assay was analyzed by Zhongshan Pharmass Corporation, Guangzhou, China. Caco-2 cells were obtained from the Institute of Basic Medical Sciences, Chinese Academy of Medical Sciences, and maintained in DMEM(H) containing 10% FBS, 400 mM L-glutamine, 4.5 mg/mL glucose, and 100 mg/mL penicillin and streptomycin. Caco-2 cells were cultured at 37 °C in a 5% CO<sub>2</sub> and 90% relative humidity environment. Cells were used between passages 20 and 40. After 21 days of culture, the proper formation of monolayer was verified by measuring the transepithelial electrical resistance (TEER). Drug transport from the apical side to the basolateral side (A→B) and from the basolateral side to the apical side (A→B) was measured

under the same conditions. To verify this model, digoxin was used as the positive control for P-gp-mediated drug efflux. All assays were performed with compounds at a concentration of 10 μM for 1 h. After the monolayer was washed with HBSS three times, the compounds were diluted and added to the appropriate well (pH 6.8 for apical side and pH 7.4 for basolateral side). The plate was incubated at 37 °C for 60 min. Samples were collected from the donor side and from the receiver side. The concentration of samples was measured by HPLC-MS/MS (API 4000 Q-Trap). The apparent permeability ( $P_{app}$ ) is expressed using the following equation:  $P_{app} = (\Delta Q/\Delta t)/C_0 A$ , where  $\Delta Q/\Delta t$  is the rate of permeation,  $C_0$  is initial concentration, and  $A$  is the monolayer area. For bidirectional permeability, the efflux ratio was defined as  $P_{app}(B \rightarrow A)/P_{app}(A \rightarrow B)$ . High efflux ratio (>3) indicates that a compound is a potential substrate for P-gp or other active transport systems.

## ■ ASSOCIATED CONTENT

### S Supporting Information

The Supporting Information is available free of charge via the Internet at The Supporting Information is available free of charge on the ACS Publications website at DOI: [10.1021/acs.jmedchem.5b01511](https://doi.org/10.1021/acs.jmedchem.5b01511).

Virtual screening results and primary biological evaluation, statistics of the data sets and structure refinement, chemistry part of synthesis and characterization, molecular dynamic simulation, and ligand density contour from X-ray crystallography (PDF)

Molecular formula strings for target compounds with associated biochemical and biological data (CSV)

### Accession Codes

Coordinates for 11 compounds have been deposited with the Protein Data Bank under the following accession codes: **17** (5CPS), **19** (5CRM), **28** (5CQT), **29** (5CPE), **36** (5COI), **42** (5D0C), **58** (5CY9), **67** (5CTL), **71** (5CRZ), **80** (5CS8), and **85** (5DX4).

## ■ AUTHOR INFORMATION

### Corresponding Author

\*Phone: 86-20-32093612. E-mail: [xu\\_yong@gibh.ac.cn](mailto:xu_yong@gibh.ac.cn).

### Author Contributions

||X.X., Y.Z., and Z. L. contributed equally to this work.

### Notes

The authors declare no competing financial interest.

## ■ ACKNOWLEDGMENTS

We gratefully acknowledge financial support from the National Natural Science Foundation of China (grant 81373325), the National Key Basic Research Program of China (973 Program, grant 2013CB910601), the “100 Talents Project” of CAS, Natural Science Foundation of Guangdong province (grant c15140600000016), and the “Interdisciplinary Cooperation Team” Program for Science and Technology Innovation of the CAS. We thank the staff members at beamline BL17U1 of the Shanghai Synchrotron Radiation Facility of China for support in the diffraction data collection. We also thank the staff of BL19U1 beamline at National Center for Protein Sciences Shanghai and Shanghai Synchrotron Radiation Facility, Shanghai, People’s Republic of China, for assistance during data collection. We gratefully acknowledge support from the Guangzhou Branch of the Supercomputing Center of Chinese Academy of Sciences.

## ABBREVIATIONS USED

HATs, histone acetyltransferases; HDACs, histone deacetylases; BRD, bromodomain; BET, bromodomain and extra-terminal domain; SBVS, structure-based virtual screening; BRD4(1), first bromodomain of BRD4 RMSD; SAR, structure–activity relationship; KAc, acetylated lysine; TSA, thermal stability shift assay; ITC, isothermal titration calorimetry

## REFERENCES

- (1) Arrowsmith, C. H.; Bountra, C.; Fish, P. V.; Lee, K.; Schapira, M. Epigenetic protein families: a new frontier for drug discovery. *Nat. Rev. Drug Discovery* **2012**, *11*, 384–400.
- (2) Filippakopoulos, P.; Picaud, S.; Mangos, M.; Keates, T.; Lambert, J. P.; Barsyte-Lovejoy, D.; Felletar, I.; Volkmer, R.; Muller, S.; Pawson, T.; Gingras, A. C.; Arrowsmith, C. H.; Knapp, S. Histone recognition and large-scale structural analysis of the human bromodomain family. *Cell* **2012**, *149*, 214–231.
- (3) Zeng, L.; Zhou, M. M. Bromodomain: an acetyl-lysine binding domain. *FEBS Lett.* **2002**, *513*, 124–128.
- (4) Filippakopoulos, P.; Knapp, S. The bromodomain interaction module. *FEBS Lett.* **2012**, *586*, 2692–2704.
- (5) Tamkun, J. W.; Deuring, R.; Scott, M. P.; Kissinger, M.; Pattatucci, A. M.; Kaufman, T. C.; Kennison, J. A. brahma: a regulator of *Drosophila* homeotic genes structurally related to the yeast transcriptional activator SNF2/SWI2. *Cell* **1992**, *68*, 561–572.
- (6) Vidler, L. R.; Brown, N.; Knapp, S.; Hoelder, S. Druggability analysis and structural classification of bromodomain acetyl-lysine binding sites. *J. Med. Chem.* **2012**, *55*, 7346–7359.
- (7) Zeng, L.; Li, J.; Muller, M.; Yan, S.; Mujtaba, S.; Pan, C.; Wang, Z.; Zhou, M. M. Selective small molecules blocking HIV-1 Tat and coactivator PCAF association. *J. Am. Chem. Soc.* **2005**, *127*, 2376–2377.
- (8) Filippakopoulos, P.; Qi, J.; Picaud, S.; Shen, Y.; Smith, W. B.; Fedorov, O.; Morse, E. M.; Keates, T.; Hickman, T. T.; Felletar, I.; Philpott, M.; Munro, S.; McKeown, M. R.; Wang, Y.; Christie, A. L.; West, N.; Cameron, M. J.; Schwartz, B.; Heightman, T. D.; La Thangue, N.; French, C. A.; Wiest, O.; Kung, A. L.; Knapp, S.; Bradner, J. E. Selective inhibition of BET bromodomains. *Nature* **2010**, *468*, 1067–1073.
- (9) Muller, S.; Knapp, S. Discovery of BET bromodomain inhibitors and their role in target validation. *MedChemComm* **2014**, *5*, 288–296.
- (10) Muller, S.; Filippakopoulos, P.; Knapp, S. Bromodomains as therapeutic targets. *Expert Rev. Mol. Med.* **2011**, *13*, e29.
- (11) Matzuk, M. M.; McKeown, M. R.; Filippakopoulos, P.; Li, Q.; Ma, L.; Agno, J. E.; Lemieux, M. E.; Picaud, S.; Yu, R. N.; Qi, J.; Knapp, S.; Bradner, J. E. Small-molecule inhibition of BRDT for male contraception. *Cell* **2012**, *150*, 673–684.
- (12) Drouin, L.; McGrath, S.; Vidler, L. R.; Chaikud, A.; Monteiro, O.; Tallant, C.; Philpott, M.; Rogers, C.; Fedorov, O.; Liu, M.; Akhtar, W.; Hayes, A.; Raynaud, F.; Muller, S.; Knapp, S.; Hoelder, S. Structure enabled design of BAZ2-ICR, a chemical probe targeting the bromodomains of BAZ2A and BAZ2B. *J. Med. Chem.* **2015**, *58*, 2553–2559.
- (13) Picaud, S.; Da Costa, D.; Thanasiopoulos, A.; Filippakopoulos, P.; Fish, P. V.; Philpott, M.; Fedorov, O.; Brennan, P.; Bunnage, M. E.; Owen, D. R.; Bradner, J. E.; Taniere, P.; O'Sullivan, B.; Muller, S.; Schwaller, J.; Stankovic, T.; Knapp, S. PFI-1, a highly selective protein interaction inhibitor, targeting BET Bromodomains. *Cancer Res.* **2013**, *73*, 3336–3346.
- (14) Rooney, T. P.; Filippakopoulos, P.; Fedorov, O.; Picaud, S.; Cortopassi, W. A.; Hay, D. A.; Martin, S.; Tumber, A.; Rogers, C. M.; Philpott, M.; Wang, M.; Thompson, A. L.; Heightman, T. D.; Pryde, D. C.; Cook, A.; Paton, R. S.; Muller, S.; Knapp, S.; Brennan, P. E.; Conway, S. J. A series of potent CREBBP bromodomain ligands reveals an induced-fit pocket stabilized by a cation-pi interaction. *Angew. Chem., Int. Ed.* **2014**, *53*, 6126–6130.
- (15) Picaud, S.; Wells, C.; Felletar, I.; Brotherton, D.; Martin, S.; Savitsky, P.; Diez-Dacal, B.; Philpott, M.; Bountra, C.; Lingard, H.; Fedorov, O.; Muller, S.; Brennan, P. E.; Knapp, S.; Filippakopoulos, P. RVX-208, an inhibitor of BET transcriptional regulators with selectivity for the second bromodomain. *Proc. Natl. Acad. Sci. U. S. A.* **2013**, *110*, 19754–19759.
- (16) Ran, X.; Zhao, Y.; Liu, L.; Bai, L.; Yang, C. Y.; Zhou, B.; Meagher, J. L.; Chinnaswamy, K.; Stuckey, J. A.; Wang, S. Structure-based design of gamma-carboline analogues as potent and specific BET bromodomain inhibitors. *J. Med. Chem.* **2015**, *58*, 4927–4939.
- (17) Brand, M.; Measures, A. M.; Wilson, B. G.; Cortopassi, W. A.; Alexander, R.; Hoss, M.; Hewings, D. S.; Rooney, T. P.; Paton, R. S.; Conway, S. J. Small molecule inhibitors of bromodomain-acetyl-lysine interactions. *ACS Chem. Biol.* **2015**, *10*, 22–39.
- (18) Hay, D.; Fedorov, O.; Filippakopoulos, P.; Martin, S.; Philpott, M.; Picaud, S.; Hewings, D. S.; Uttakar, S.; Heightman, T. D.; Conway, S. J.; Knapp, S.; Brennan, P. E. The design and synthesis of 5-and 6-isoxazolylbenzimidazoles as selective inhibitors of the BET bromodomains. *MedChemComm* **2013**, *4*, 140–144.
- (19) Hammitzsch, A.; Tallant, C.; Fedorov, O.; O'Mahony, A.; Brennan, P. E.; Hay, D. A.; Martinez, F. O.; Al-Mossawi, M. H.; de Wit, J.; Vecellio, M.; Wells, C.; Wordsworth, P.; Muller, S.; Knapp, S.; Bowness, P. CBP30, a selective CBP/p300 bromodomain inhibitor, suppresses human Th17 responses. *Proc. Natl. Acad. Sci. U. S. A.* **2015**, *112*, 10768–10733.
- (20) Xu, M.; Unzue, A.; Dong, J.; Spiliotopoulos, D.; Nevado, C.; Caflisch, A. Discovery of CREBBP bromodomain inhibitors by high-throughput docking and hit optimization guided by molecular dynamics. *J. Med. Chem.* **2016**, *59*, 10.1021/acs.jmedchem.5b00171.
- (21) Gosmini, R.; Nguyen, V. L.; Toum, J.; Simon, C.; Brusq, J. M.; Krysa, G.; Mirguet, O.; Riou-Eymard, A. M.; Boursier, E. V.; Trottet, L.; Bamborough, P.; Clark, H.; Chung, C. W.; Cutler, L.; Demont, E. H.; Kaur, R.; Lewis, A. J.; Schilling, M. B.; Soden, P. E.; Taylor, S.; Walker, A. L.; Walker, M. D.; Prinjha, R. K.; Nicodeme, E. The discovery of I-BET726 (GSK1324726A), a potent tetrahydroquinoline ApoA1 up-regulator and selective BET bromodomain inhibitor. *J. Med. Chem.* **2014**, *57*, 8111–8131.
- (22) Nicodeme, E.; Jeffrey, K. L.; Schaefer, U.; Beinke, S.; Dewell, S.; Chung, C. W.; Chandwani, R.; Marazzi, I.; Wilson, P.; Coste, H.; White, J.; Kirilovsky, J.; Rice, C. M.; Lora, J. M.; Prinjha, R. K.; Lee, K.; Tarakhovsky, A. Suppression of inflammation by a synthetic histone mimic. *Nature* **2010**, *468*, 1119–1123.
- (23) Mirguet, O.; Lamotte, Y.; Donche, F.; Toum, J.; Gellibert, F.; Bouillot, A.; Gosmini, R.; Nguyen, V. L.; Delannee, D.; Seal, J.; Blandel, F.; Boullay, A. B.; Boursier, E.; Martin, S.; Brusq, J. M.; Krysa, G.; Riou, A.; Tellier, R.; Costaz, A.; Huet, P.; Dudit, Y.; Trottet, L.; Kirilovsky, J.; Nicodeme, E. From ApoA1 upregulation to BET family bromodomain inhibition: discovery of I-BET151. *Bioorg. Med. Chem. Lett.* **2012**, *22*, 2963–2967.
- (24) Seal, J.; Lamotte, Y.; Donche, F.; Bouillot, A.; Mirguet, O.; Gellibert, F.; Nicodeme, E.; Krysa, G.; Kirilovsky, J.; Beinke, S.; McCleary, S.; Rioja, I.; Bamborough, P.; Chung, C. W.; Gordon, L.; Lewis, T.; Walker, A. L.; Cutler, L.; Lugo, D.; Wilson, D. M.; Witherington, J.; Lee, K.; Prinjha, R. K. Identification of a novel series of BET family bromodomain inhibitors: binding mode and profile of I-BET151 (GSK1210151A). *Bioorg. Med. Chem. Lett.* **2012**, *22*, 2968–2972.
- (25) Fish, P. V.; Filippakopoulos, P.; Bish, G.; Brennan, P. E.; Bunnage, M. E.; Cook, A. S.; Federov, O.; Gerstenberger, B. S.; Jones, H.; Knapp, S.; Marsden, B.; Nocka, K.; Owen, D. R.; Philpott, M.; Picaud, S.; Primiano, M. J.; Ralph, M. J.; Sciammetta, N.; Trzupek, J. D. Identification of a chemical probe for bromo and extra C-terminal bromodomain inhibition through optimization of a fragment-derived hit. *J. Med. Chem.* **2012**, *55*, 9831–9837.
- (26) Chung, C. W.; Dean, A. W.; Woolven, J. M.; Bamborough, P. Fragment-based discovery of bromodomain inhibitors part 1: inhibitor binding modes and implications for lead discovery. *J. Med. Chem.* **2012**, *55*, 576–586.

- (27) Bamborough, P.; Diallo, H.; Goodacre, J. D.; Gordon, L.; Lewis, A.; Seal, J. T.; Wilson, D. M.; Woodrow, M. D.; Chung, C. W. Fragment-based discovery of bromodomain inhibitors part 2: optimization of phenylisoxazole sulfonamides. *J. Med. Chem.* **2012**, *55*, 587–596.
- (28) Zhao, L.; Wang, Y.; Cao, D.; Chen, T.; Wang, Q.; Li, Y.; Xu, Y.; Zhang, N.; Wang, X.; Chen, D.; Chen, L.; Chen, Y. L.; Xia, G.; Shi, Z.; Liu, Y. C.; Lin, Y.; Miao, Z.; Shen, J.; Xiong, B. Fragment-based drug discovery of 2-thiazolidinones as BRD4 inhibitors: 2. Structure-based optimization. *J. Med. Chem.* **2015**, *58*, 1281–1297.
- (29) Zhao, L.; Cao, D.; Chen, T.; Wang, Y.; Miao, Z.; Xu, Y.; Chen, W.; Wang, X.; Li, Y.; Du, Z.; Xiong, B.; Li, J.; Xu, C.; Zhang, N.; He, J.; Shen, J. Fragment-based drug discovery of 2-thiazolidinones as inhibitors of the histone reader BRD4 bromodomain. *J. Med. Chem.* **2013**, *56*, 3833–3851.
- (30) Gehling, V. S.; Hewitt, M. C.; Vaswani, R. G.; Leblanc, Y.; Cote, A.; Nasveschuk, C. G.; Taylor, A. M.; Harmange, J. C.; Audia, J. E.; Pardo, E.; Joshi, S.; Sandy, P.; Mertz, J. A.; Sims, R. J., 3rd; Bergeron, L.; Bryant, B. M.; Bellon, S.; Poy, F.; Jayaram, H.; Sankaranarayanan, R.; Yellapantula, S.; Bangalore Srinivasamurthy, N.; Birudukota, S.; Albrecht, B. K. Discovery, design, and optimization of isoxazole azepine BET inhibitors. *ACS Med. Chem. Lett.* **2013**, *4*, 835–840.
- (31) Basheer, F.; Huntly, B. J. BET bromodomain inhibitors in leukemia. *Exp. Hematol.* **2015**, *43*, 718–731.
- (32) Filippakopoulos, P.; Knapp, S. Targeting bromodomains: epigenetic readers of lysine acetylation. *Nat. Rev. Drug Discovery* **2014**, *13*, 337–356.
- (33) Zhang, Y.; Xue, X.; Jin, X.; Song, Y.; Li, J.; Luo, X.; Song, M.; Yan, W.; Song, H.; Xu, Y. Discovery of 2-oxo-1,2-dihydrobenzo[cd]-indole-6-sulfonamide derivatives as new ROR $\gamma$  inhibitors using virtual screening, synthesis and biological evaluation. *Eur. J. Med. Chem.* **2014**, *78*, 431–441.
- (34) Melcher, K.; Xu, Y.; Ng, L. M.; Zhou, X. E.; Soon, F. F.; Chinnusamy, V.; Suino-Powell, K. M.; Kovach, A.; Tham, F. S.; Cutler, S. R.; Li, J.; Yong, E. L.; Zhu, J. K.; Xu, H. E. Identification and mechanism of ABA receptor antagonism. *Nat. Struct. Mol. Biol.* **2010**, *17*, 1102–1108.
- (35) Fedorov, O.; Lingard, H.; Wells, C.; Monteiro, O. P.; Picaud, S.; Keates, T.; Yapp, C.; Philpott, M.; Martin, S. J.; Felletar, I.; Marsden, B. D.; Filippakopoulos, P.; Muller, S.; Knapp, S.; Brennan, P. E. [1,2,4]triazolo[4,3-a]phthalazines: inhibitors of diverse bromodomains. *J. Med. Chem.* **2014**, *57*, 462–476.
- (36) Leslie, A. G.; Powell, H. R. Processing diffraction data with mosflm. *Evol. Dev.* **2007**, *24*, 41–51.
- (37) Collaborative computational project. the CCP4 suite: programs for protein crystallography. *Acta Crystallogr., Sect. D: Biol. Crystallogr.* **1994**, *50*, 760–763.
- (38) McCoy, A. J.; Grosse-Kunstleve, R. W.; Adams, P. D.; Winn, M. D.; Storoni, L. C.; Read, R. J. Phaser crystallographic software. *J. Appl. Crystallogr.* **2007**, *40*, 658–674.
- (39) Murshudov, G. N.; Skubak, P.; Lebedev, A. A.; Pannu, N. S.; Steiner, R. A.; Nicholls, R. A.; Winn, M. D.; Long, F.; Vagin, A. A. REFMAC5 for the refinement of macromolecular crystal structures. *Acta Crystallogr., Sect. D: Biol. Crystallogr.* **2011**, *67*, 355–367.
- (40) Emsley, P.; Cowtan, K. Coot: model-building tools for molecular graphics. *Acta Crystallogr., Sect. D: Biol. Crystallogr.* **2004**, *60*, 2126–2132.
- (41) Chen, V. B.; Arendall, W. B., 3rd; Headd, J. J.; Keedy, D. A.; Immormino, R. M.; Kapral, G. J.; Murray, L. W.; Richardson, J. S.; Richardson, D. C. MolProbity: all-atom structure validation for macromolecular crystallography. *Acta Crystallogr., Sect. D: Biol. Crystallogr.* **2010**, *66*, 12–21.
- (42) DeLano, W. L. *The PyMOL Molecular Graphics System*; DeLano Scientific LLC: Palo Alto, CA, 2002.